Modelling rock glacier ice content based on InSAR-derived velocity, Khumbu and Lhotse Valleys, Nepal

Yan Hu[1,2,3], Stephan Harrison[2], Lin Liu[1,3], Joanne Laura Wood[2]

[1]Earth System Science Programme, Faculty of Science, The Chinese University of Hong Kong, Hong Kong SAR, China
5   [2]College of Life and Environmental Sciences, University of Exeter, Penryn, Cornwall, TR10 9EZ, UK
[3]Institute of Environment, Energy and Sustainability, The Chinese University of Hong Kong, The Chinese University of Hong Kong, Hong Kong SAR, China

Correspondence to: Yan Hu (huyan@link.cuhk.edu.hk)

10   **Abstract.** Active rock glaciers are viscous flow features embodying ice-rich permafrost and other ice masses. They contain significant amounts of ground ice and serve as potential freshwater reservoirs as mountain glaciers melt in response to climate warming. However, current knowledge about ice content in rock glaciers has been acquired mainly from in situ investigations in limited study areas, which hinders a comprehensive understanding of ice storage in rock glaciers situated in remote mountains over local to regional scales. This study proposes a novel approach for assessing the hydrological value of rock
15   glaciers in a more quantitative way and presents exploratory results focusing on a small region. We develop an empirical rheological model to infer ice content of rock glaciers using readily available input data, including rock glacier planar shape, surface slope angle, active layer thickness, and surface velocity. The model is calibrated and validated using observational data from the Chilean Andes and the Swiss Alps. We apply the model to five rock glaciers in Khumbu and Lhotse Valleys, north-eastern Nepal. The velocity constraints applied to the model are derived from Interferometric Synthetic Aperture Radar
20   (InSAR) measurements. The volume of rock glacier is estimated based on an existing scaling approach. The inferred volumetric ice fraction in Khumbu and Lhotse Valleys ranges from 70±8% to 74±8%; and the water volume equivalents lie between 1.4±0.2 to 5.9±0.6 million m^3 for the coherently moving parts of individual ~~landforms.~~ Due to the accessibility of model inputs, our approach is applicable to permafrost regions where observational data are lacking~~, and is thus~~ valuable for estimating the water storage potential of rock glaciers in remote areas.

25   **1 Introduction**

Rock glaciers are valley-floor and valley-side landforms that commonly occur in the glacial and periglacial realm. Intact rock glaciers ~~develop permafrost or glacial ice cores~~ containing considerable amount of ground ice (Ballantyne, 2018; Berthling, 2011; Brenning, 2005a). Recent research has suggested that they represent important hydrological reservoirs in areas where glaciers are undergoing recession in the face of climate change, such as South America (Azócar and Brenning, 2010;
30   Rangecroft et al., 2014), North America (Munroe, 2018), and South Asia East (Jones et al., 2018a). Corte (1976) first proposed

the potential hydrological value of rock glaciers, yet research on the role of rock glaciers in maintaining hydrological stores in mountain catchments remains limited.

Jones et al. (2021) were the first to show that around 25,000 rock glaciers exist in the Himalayas, covering 3747 km² and containing 51.80 ± 10.36 km³ of water volume equivalent. The ratio between rock glacier ice content and that in glaciers in the region was 1:25, ranging from 1:42 to 1:17 in the Eastern and Central Himalaya and falling to 1:9 in Nepal. Importantly, we expect these existing ratios to reduce significantly as glaciers melt and/or undergo transitions to rock glaciers. Few studies have investigated the hydrological contribution of rock glaciers to surface runoffs at annual or seasonal timescale (e.g., Geiger et al., 2014; Harrington et al., 2018; Krainer and Mostler, 2002; Winkler et al., 2016), and little evidence has shown that rock glacier discharge is a prominent water source at present due to the insulation effect produced by their blocky surfaces (Duguay et al., 2015; Jones et al., 2019b; Pruessner et al., 2021). Yet, on multi-annual to centennial and millennial timescales, we expect rock glaciers with high ice content to serve as water reservoirs long after glaciers have melted.

To date, we have little quantitative information concerning the ice content of rock glaciers, which hinders our understanding of the potential future hydrological role of rock glaciers. Currently, estimates of ice content in rock glaciers have focused on empirical information from drilling cores and boreholes (e.g., Hausmann et al., 2007; Arenson et al., 2002; Berthling et al., 2000; Croce and Milana, 2002; Guglielmin et al., 2004; Haeberli et al., 1998; Krainer et al., 2015; Leopold et al., 2011; Steig et al., 1998), and from geophysical surveys (e.g., for reviews see: Hauck, 2013; Kneisel et al., 2008; Scott et al., 1990). However, these approaches to estimate the likely ice content are costly, time-consuming, and labour-intensive to apply to rock glaciers at high altitudes and in remote mountains. It is therefore desirable to develop alternative approaches to understanding the likely ice content of rock glaciers, especially for regional scale estimates.

Ice content is one factor controlling the movement of rock glaciers by influencing the driving force and the rheological properties of materials which constitute the permafrost core (Arenson and Springman, 2005a; Cicoira et al., 2020), in addition to other properties including ground temperature, sub-surface structure, debris content, and water pressure (Moore, 2014), thus it is feasible to infer ice content using rheological modelling and observed kinematic data. Here we adapt an empirical model by integrating rheological properties of rock glaciers derived from laboratory experiments (Arenson and Springman, 2005a), and parameterise the rheological model based on the structure and composition data of Las Liebres rock glacier (Monnier and Kinnard, 2015b; Monnier and Kinnard, 2016). We then apply the model to simulate surface velocities of three rock glaciers with known ice content in the Swiss Alps and evaluate the modelling results to determine a suitable parameterisation scheme. Finally, we apply the calibrated model for five rock glaciers in the study area of north-eastern Nepal and model their ice contents based on remote-sensing-derived downslope velocities as constraints.

2 Study area

Khumbu and Lhotse valleys are located in north-eastern Nepal (Fig. 1a). Among the highest in the world, the Khumbu and Lhotse glaciers draining Everest have well defined debris-covered snouts. The tributary valleys contain a variety of rock glaciers and composite landforms where glaciers are transitioning to rock glaciers (Jones et al., 2019; Knight et al., 2019).

2

There are five rock glaciers in the study area, namely Kala-Patthar, Kongma, Lingten, Nuptse, and Tobuche (Fig. 1b). The five

65   rock glaciers examined in this study are situated at 4900–5090 m a.s.l., near the lower limit of permafrost in the region. Previous seismic refraction surveys conducted on active rock glaciers indicate that the lower limit of permafrost occurrence in this region to be ~5000–5300 m a.s.l. (Jakob, 1992; Fukui et al., 2007), which is consistent with an earlier estimate of 4900 m a.s.l. based on ground temperature measurements (Fujii and Higuchi, 1976).

Meteorological data provided by the Pyramid Observatory Laboratory near Lobuche village on the western side of the Khumbu

70   Glacier (5050 m a.s.l.) reveal that the dominating climate of this area is the South Asian Summer Monsoon. For the period of 1994–2013, recorded accumulated annual precipitation was 449 mm yr^{-1}, with 90% of the precipitation concentrated during June–September (Salerno et al., 2015). The mean annual air temperature is –2.4 °C (Salerno et al., 2015).

Measurements of ground temperature in the study area are scarce in general. However, we infer that these rock glaciers develop in a warm permafrost environment for the following reasons: (1) ~~the landforms~~ are located near or below the altitudinal limit

75   of permafrost distribution in Nepal (Fujii and Higuchi, 1976; Jakob, 1992), indicating that the local environment is at the critical limit of permafrost occurrence; (2) based on empirical relationships between mean annual ground temperature (MAGT), mean annual air temperature, latitude, and altitude, the estimated MAGT is >0.5°C, which suggests that permafrost in this area is in a warm and unstable state (Nan et al., 2002; Zhao and Sheng, 2015).
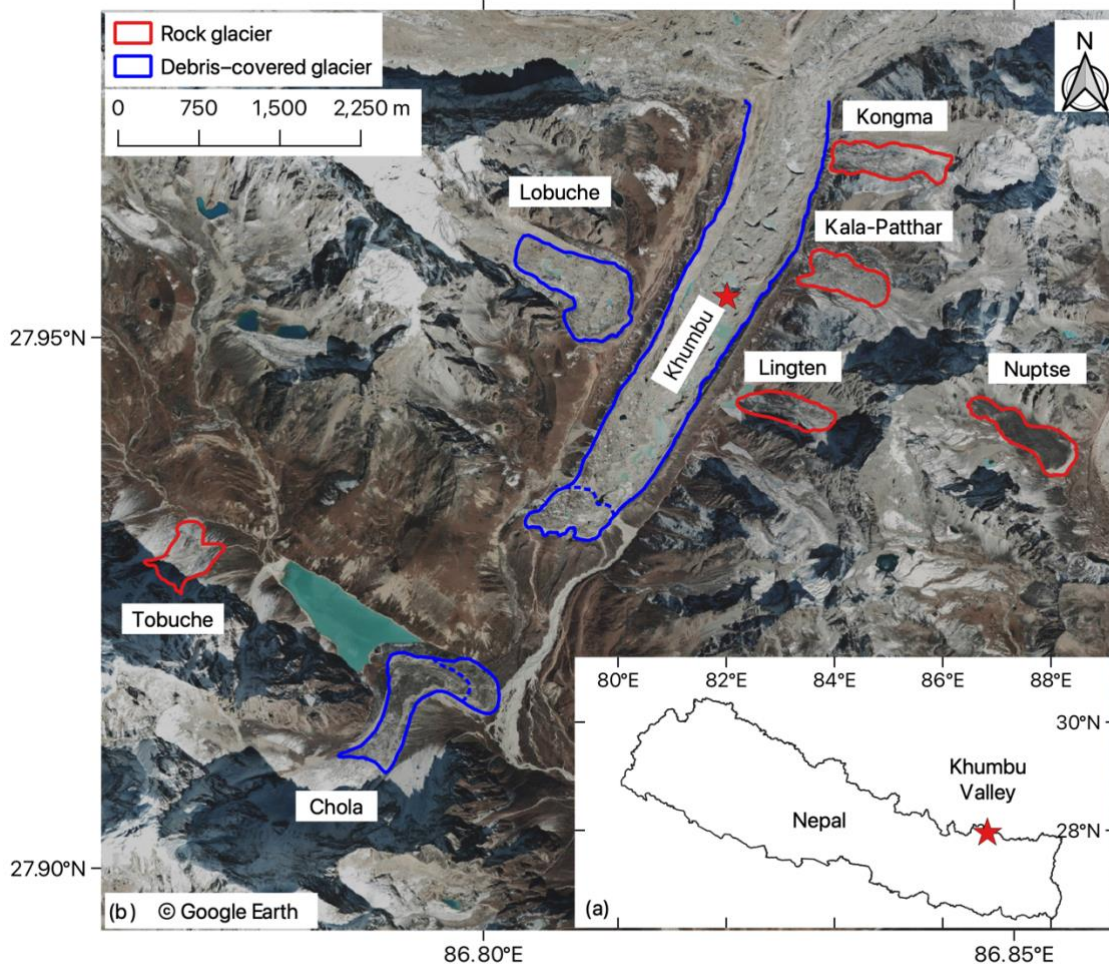
Figure 1: (a) Location of the study site; (b) Google Earth images (taken in 2019) showing the spatial distribution of the active ~~ice-debris landforms, including~~ rock glaciers (RG) in red outlines and debris-covered glaciers (DCG) in blue boundaries. The RGs are delineated by Jones et al. (2018) and the DCGs by the authors based on Google Earth images. The termini of Khumbu and Chola DCGs (outlined by dotted lines) are transitioning into rock glaciers (Knight et al., 2019).

3 Methods

The main workflow of our method is illustrated in Fig.2. In this section, we first introduce the model design and basic assumptions we adopted (Sect. 3.1). Then we present the following development steps in sequence: model calibration (Sect. 3.2), validation (Sect. 3.3), and sensitivity test (Sect. 3.4). Finally, we describe ~~the model application based on InSAR~~ (Sect. 3.5).
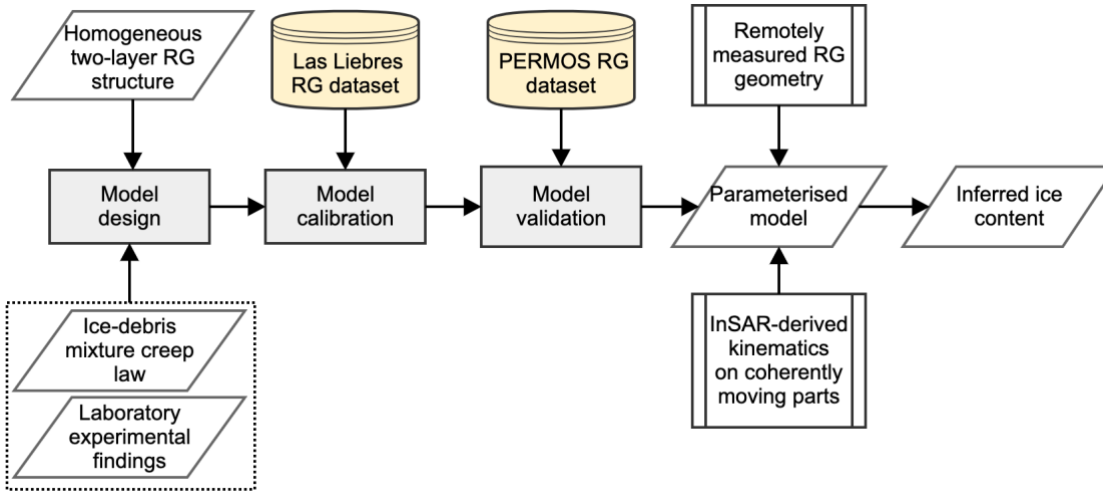
90

Figure 2: Diagram of the workflow conducted in this study to develop and apply a modelling approach for inferring ice content of rock glaciers (RG).

3.1 Model design and assumptions

Active rock glaciers are viscous flow features embodying ice-rich permafrost (Ballantyne, 2018; Berthling, 2011; Haeberli,

95   2000). Many previous modelling studies depict the deformation mechanism of rock glaciers based on Glen's flow law (e.g., Arenson and Springman, 2005a; Cicoira et al., 2020; Whalley and Azizi, 1994), which essentially relates strain rate ($\dot{\varepsilon}$) with effective shear stress (τ) and describes the rheology of ice flow (Glen, 1955):

$$\dot{\varepsilon} = A\tau^n ,\tag{1}$$

where A and n are creep parameters reflecting variations in environmental conditions (mainly temperature and pressure),

100   material properties (such as composition, structure, and texture), and operating creep mechanisms (e.g., diffusion and dislocation).

In this study, we primarily adopted a creep model of ice–debris mixture, proposed by Moore (2014), based on Glen's flow law:

$$\dot{\varepsilon} = EA[(\tau - \tau_{th})\Gamma]^n ,\tag{2}$$

where E is a strain enhancement factor; Γ is a parameter reflecting the strength of the ice–debris mixture, associated with the

105   volumetric debris content (θ_d). We assumed the rock glacier has an ice-rich permafrost core. When θ_d is less than a critical volumetric debris content (θ_{dc}), ice creep dominates the behaviour of the mixture , and the value of Γ equals one. Theoretically, θ_{dc} is around 0.52 (Moore, 2014). τ is the driving stress and τ_{th} is a threshold stress imparted by the frictional strength between debris particles, also depending upon the volumetric debris content (θ_d).

Assuming that $\tau_{th} \ll \tau$, $\theta_d < \theta_{dc}$, and $\Gamma = 1$, Eq. 2 can be reduced to the following form (Monnier and Kinnard, 2016):

110    $$\dot{\varepsilon} = \left(\frac{\tau}{B}\right)^n ,\tag{3}$$

5

where B is the effective viscosity and is equal to $\left(\frac{1}{EA}\right)^{-\frac{1}{n}}$. We introduced the effective viscosity (B) to absorb the intricate effects of strain enhancement factor (E), threshold stress (τ_{th}), and most importantly, the creep parameter (A), which is primarily affected by ground temperatures (Mellor and Testa, 1969). Previous research (e.g., Arenson and Springman, 2005a; Azizi and Whalley, 1996; Kääb et al., 2007; Ladanyi, 2003) considered this factor by implementing a heat diffusion model

115 (proposed by Carslaw and Jaeger, 1959). In this study, we used a constant effective viscosity (B) to describe the deformation behaviour of rock glaciers in a warm permafrost environment (> -3°C). The empirical formula was developed based on existing observational data and laboratory findings. This warm ground condition is likely to be realistic in our study area (Sect. 2) and occurs in the rock glaciers in the Andes and Swiss Alps selected for model calibration and validation (Sect. 3.2 and 3.3).

We assume a homogeneous structure and consider each rock glacier as a slab with uniform width and thickness and a semi-

120 elliptical cross-section, resting on a bed of constant slope, which is a common setup in glaciology (Cuffey and Paterson, 2010). It consists of two layers: an active layer and a permafrost core. The active layer is a mixture of debris and air, and the permafrost core consists of ice, unfrozen water, debris and air. Both layers are assumed as homogeneous. Movement of rock glaciers is caused by the steady creep of the permafrost core in the plane parallel to the bed slope. The active layer moves passively along with the inner core, which has been validated by observations (Arenson et al., 2002; Haeberli, 2000).

125 Here we neglected the presence of shear horizon where deformation is enhanced and ground ice content is low, as discovered from borehole investigations (Arenson et al., 2002; Buchli et al., 2018; Haeberli et al., 1998). Field observations and numerical modelling suggest that unfrozen water within the shear horizon plays an important role in controlling the seasonal variations in rock glacier creep (e.g., Buchli et al., 2018; Cicoira et al., 2019b; Kenner et al., 2019; Wirz et al., 2016). However, the short-term rock glacier kinematic patterns are irrelevant to this study focusing on modelling the relationship between ice content and

130 multi-annual average movement velocity ~~in our study~~.

From Eq. 3 and the structure and geometry illustrated in Fig. 3, we have:

$$\frac{du}{dz} = 2\left(\frac{\tau}{B}\right)^n , \tag{4}$$

where $\frac{du}{dz}$ is the velocity derivative relative to the depth z in the permafrost core.

At a given depth z, the driving stress τ is imparted, taking into account the loading of the above material and the effect of

135 frictional drag occurring between the lateral margins and surrounding bedrocks, which is represented by a shape factor S_f (Cuffey and Paterson, 2010):

$$\tau(z) = S_f \sin\alpha(\rho_{al}gh_{al} + \rho_{core}gz) , \tag{5}$$

where α is the slope angle; g is the gravitational acceleration; ρ_{al} and ρ_{core} are the densities of the active layer and the permafrost core, respectively; h_{al} is the active layer thickness.

140 The shape factor is expressed as (Oerlemans, 2001):

$$S_f = \frac{\pi}{2}\arctan\left(\frac{W}{2T}\right) , \tag{6}$$

where W and T are the width and thickness of the rock glacier, respectively.

The integration of the velocity profile (Eq. 4 and 5) is expressed as:

$$\int_0^z du = -2\left(\frac{S_f g \sin\alpha}{B}\right)^n \int_0^z (\rho_{al} h_{al} + \rho_{core} z)^n dz, \tag{7}$$

$$u(z) = u_s - \frac{2(\rho_{al} h_{al} + \rho_{core} z)^{n+1}}{\rho_{core}(n+1)}\left(\frac{S_f g \sin\alpha}{B}\right)^n, \tag{8}$$

where u_s is the surface velocity as illustrated in Fig. 3. When z is set as the thickness of the ice core (h_{core}) and basal sliding is assumed to be absent, u_s is then expressed as:

$$u_s = \frac{2(\rho_{al} h_{al} + \rho_{core} h_{core})^{n+1}}{\rho_{core}(n+1)}\left(\frac{S_f g \sin\alpha}{B}\right)^n, \tag{9}$$

The densities of the active layer (ρ_{al}) and the permafrost core (ρ_{core}) are given as:

$$\rho_{al} = \theta_{d,al}\rho_d + \theta_{a,al}\rho_a, \tag{10}$$

$$\rho_{core} = \theta_{d,core}\rho_d + \theta_{a,core}\rho_a + \theta_{i,core}\rho_i + \theta_{w,core}\rho_w, \tag{11}$$

where $\theta_{d,al}$ and $\theta_{a,al}$ are the volumetric contents of debris and air in the active layer, respectively. The volumetric contents of the components in the inner core, namely debris, air, ice, and water, are expressed as $\theta_{d,core}$, $\theta_{a,core}$, $\theta_{i,core}$, and $\theta_{w,core}$, respectively. ρ_d, ρ_a, ρ_i, and ρ_w are the densities of debris, air, ice, and water, respectively.

We fixed the air content in the permafrost core as 7.5%, which is a mean value of the air fraction in ice-rich permafrost samples (Arenson and Springman, 2005b). At near 0 °C, the volumetric content of water ($\theta_{w,core}$) displays a positive correlation with the debris fraction ($\theta_{d,core}$) (Monnier and Kinnard, 2016). Thus, we determined the $\theta_{d,core}$–$\theta_{w,core}$ relationship based on the data published in Monnier and Kinnard (2015b) and assumed the constitution of the selected rock glaciers for model validation and application followed the same linear relationship (Fig. S1). The debris density (ρ_d) was given as 2450 kg/m³ (Monnier and Kinnard, 2016). The density of air (ρ_a) is determined by the elevation of each rock glacier: for instance, rock glaciers situated between 2500 m and 3500 m have an air density of 1.007 kg/m³. The ice density (ρ_i) is 916 kg/m³ and the water density (ρ_w) is 1000 kg/m³.

For the flow law exponent (n), we first used an empirical average value as assumed in modelling pure ice creep:

$$n = 3, \tag{12}$$

We also adopted a linear relationship between n and the volumetric ice content ($\theta_{i,core}$) based on laboratory experiments undertaken on borehole samples from two rock glaciers (Arenson and Springman, 2005a):

$$n = 3\theta_{i,core}, \tag{13}$$
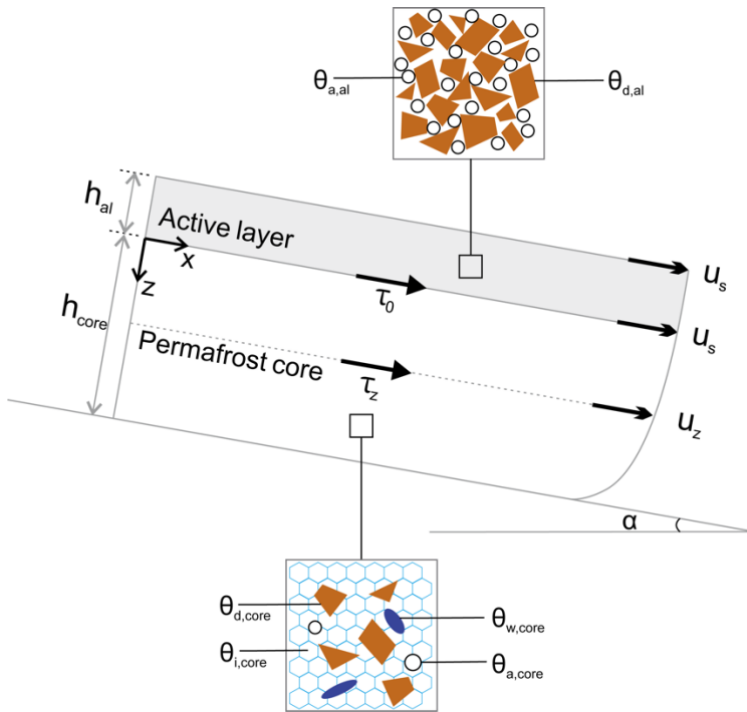
Figure 3: Schematic geometry, structure, stress status, and composition of rock glaciers (adapted from Monnier and Kinnard (2016)). The rock glacier consists of a permafrost core underlying the active layer. Parameters involved in the model include surface slope (α), active layer thickness (h_{al}), thickness of permafrost core (h_{core}), driving stress at the base of the active layer (τ_0), driving stress at depth z (τ_z), surface velocity (u_s), velocity at depth z (u_z). $\theta_{d,al}$ and $\theta_{a,al}$ refer to the debris fraction and air fraction of the active layer. $\theta_{d,core}$, $\theta_{i,core}$, $\theta_{w,core}$, and $\theta_{a,core}$ are the fractions of debris, ice, water, and air in the permafrost core, respectively.

3.2 Model calibration

Combining Eq. 9–11 with Eq. 12 or 13, we formulated several expressions depicting the relationship between the surface velocity and properties of rock glaciers, including their composition, structure, and geometry. We then calibrated the model by using observational data of Las Liebres rock glacier in Central Chilean Andes (Monnier and Kinnard, 2015b) to determine the curve of best fit between the effective viscosity (B) and the volumetric ice content ($\theta_{i,core}$). Las Liebres rock glacier was considered to have a near 0 °C permafrost temperature (Monnier and Kinnard, 2016), according to the borehole measurement of a nearby rock glacier (Monnier and Kinnard, 2013). The calibration dataset includes information of structure (h_{core} and h_{al}), geometry (α and S_f), and composition ($\theta_{d,core}$, $\theta_{a,core}$, $\theta_{i,core}$, and $\theta_{w,core}$), all of which were derived from Ground Penetrating Radar (GPR) measurements. Surface velocities (u_s) were provided by a Differential Global Positioning System (DGPS) along the central creep line at 14 locations on Las Liebres rock glacier (Monnier and Kinnard, 2015b & 2016). The limited amount of calibration data plays an important role in the calculation of the uncertainty associated with our approach (detailed in Sect. 5.1.1).

First, we adopted the exponential B–$\theta_{i,core}$ relationship estimated by Monnier & Kinnard (2016) with the same dataset and a constant creep parameter n (Eq. 12). Then by integrating the relationship between n and ice content (Eq. 13), we applied both

8

a 2nd-degree polynomial regression model and an exponential regression model to determine the $B - \theta_{i,core}$ relationship. The polynomial regression model is used to capture the subtle increase in effective viscosity when the ice fraction increases. This trend was also shown by Arenson and Springman (2005a) who suggested a parabolic relationship between the minimum axial creep strain rate and the volumetric ice content.

3.3 Model validation

The calibrated parameterisation schemes were validated using observational data from three rock glaciers in the Swiss Alps, namèly Murtèl-Corvatsch, Muragl, and Schafberg (Cicoira et al., 2019a; Arenson et al., 2002; Hoelzle et al., 1998). All of the selected rock glaciers have warm cores showing permafrost temperatures between -1 and 0 °C (PERMOS, 2019). We simulated the surface velocity (u_s) of each rock glacier by varying volumetric ice content ($\theta_{i,core}$) of the permafrost core. Then we compared the modelled velocity with the measured velocity from Terrestrial Geodetic Surveys (PERMOS, 2019). We then referred to the previously estimated ice content of the selected rock glaciers to validate our predicted results.

To derive the input parameters, we first outlined the boundaries of the three rock glaciers from Google Earth images (September of 2018), from which their shapes and areal extents can be extracted using Geographic Information System tools. As Muragl and Schafberg rock glaciers consist of multiple and/or overlapping lobes, in each of them we focus on a single active lobe for which borehole and composition data are available. The three rock glaciers selected for validation are tongue-shaped. An empirical relationship established by Brenning (2005b) was then applied to calculate the rock glacier thickness (T) from its areal extent (A_{rg}):

$$T = 50 A_{rg}^{0.2} \,, \tag{14}$$

where the area (A_{rg}) is in km^2. We assigned a relative uncertainty of 40% to the area parameter and considered the propagated error to the final modelling result. The width of each glacier was quantified as the width of its minimum envelop rectangle. We took the mean value of the active layer thickness obtained from borehole measurements in the PERMOS network as the input parameter h_{al} for each rock glacier. The surface slope (α) was calculated based on the SRTM DEM with a spatial resolution of ~30 m. Table 1 lists the values of the above parameters. The permafrost core thickness (h_{core}) can be obtained by subtracting h_{al} from the total thickness T calculated using Eq. 14.

We assumed the volumetric ice content ($\theta_{i,core}$) of the permafrost core to be between 40% and 100%, considering the prerequisites of the modified ice–debris mixture flow law (Eq. 3) that the debris fraction ($\theta_{d,core}$) should be less than the threshold (θ_{dc}) (Sect. 3.1). We varied the ice content ($\theta_{i,core}$) by 1% in each step to model the corresponding surface velocities (u_s).

Table 1. Summary of the geometric and structural parameters used in the validation.

Rock glacier	Area ($\mathbf{A_{rg}}$) (km^2)	Width (W) (m)	Active layer thickness ($\mathbf{h_{al}}$) (m)	Surface slope ($\mathbf{\alpha}$) (°)
Murtèl-Corvatsch	0.065	29	3.0	16
Muragl	0.027	24	4.5	12

| Schafberg | 0.027 | 24 | 4.8 | 16 |

3.4 Sensitivity analysis

To explore how uncertainties of the input parameters contribute to the final output of the developed approach, we tested the response of the model to varying input parameters by performing a series of synthetic sensitivity experiments. For these experiments, we simulated surface velocities of the rock glacier with variable ice fractions and inferred the current ice content from the velocity constraint. A reference scenario is set up with the parameters of Murtèl-Corvatsch rock glacier and labelled as Sc-1.0. We designed eight scenarios extending from Sc-1.0, naming each scenario after a multiplication factor which indicates the ratio between the applied parameter and the reference scenario; For two parameters, namely debris density (ρ_d) and debris fraction in the active layer ($\theta_{d,al}$), we applied a value range according to the known natural variability based on observations (ρ_d: 1450–3450 kg/m^3; $\theta_{d,al}$: 13–93%). A full list of the parameters used in the sensitivity test is presented in Table S1 in the supplementary materials. We performed the sensitivity experiments by varying one parameter at a time while keeping the other variables constant.

3.5 Model application

The validated model with the <mark>optimal</mark> parameterisation scheme was applied to estimate ice content of rock glaciers with remotely sensed input data. In this subsection, we present our method to ~~measure~~ surface velocities of rock glaciers ~~with~~ InSAR ~~for constraining the model~~ (Sect. 3.5.1) and use complementary remote sensing products to derive geometric and structural parameters (Sect. 3.5.2).

3.5.1 Deriving surface velocity constraints with Differential InSAR

InSAR has been widely applied to quantifying surface velocities of rock glaciers (e.g., Strozzi et al., 2004; Bertone et al., 2022; Reinosch et al., 2021; Rouyet et al., 2019). In this study, we adopted the conventional two-pass Differential InSAR method to derive the surface velocities by assuming rock glaciers creep along the slope direction (~~Brencher et al., 2021~~; ~~Hu et al., 2021;~~ Liu et al., 2013; Wang et al., 2017). We identified the coherently moving part of the rock glacier and determined the surface velocity for constraining the model.

Step 1: Interferometric processing

Nineteen L-band ALOS PALSAR images and twenty-one ALOS-2 PALSAR-2 images acquired during 2006–2010 and 2015–2020, respectively, were used to form more than fifty interferograms to measure the surface displacements of the ~~landforms in the study area~~ (Table 2). We selected interferograms to achieve high interferometric coherence by following the criteria such as: (1) short temporal spans (less than 92 days for ALOS pairs and 70 days for ALOS-2 pairs); (2) short perpendicular baselines (smaller than 800 m for ALOS pairs and 400 m for ALOS-2 pairs). We estimated and removed the topographic phase with the

1-arcsec digital elevation models (DEM) produced by the Shuttle Radar Topography Mission (SRTM) (spatial resolution ~30 m). Multi-looking operation and adaptive Goldstein filter (8×8 pixels) were applied using the open-source software ISCE version 2.4.2 (available at https://github.com/isce-framework/isce2). The final georeferenced interferograms have a ground resolution of ~30 m according to the DEM. The interferograms were unwrapped using the SNAPHU software (Chen and Zebker, 2002). We randomly selected three pixels at places, supposed to be stable near each ice–debris landform (within 300m) and averaged their phase values to re-reference the unwrapped phases measured within the landforms. By doing so, atmospheric delays can be effectively removed because these lead to long-wavelength artefacts and can be assumed as constant within the range of our study objects (Hanssen, 2001).

Step 2: Calculating downslope velocities from high-quality interferograms

We then derived the surface velocities along the SAR satellite line-of-sight (LOS) direction from the unwrapped interferograms and projected the LOS velocities onto the downslope direction of the landforms. The projection was conducted considering the satellite's flight direction, the local incidence angle, and the landform topographic parameters including the aspect and slope angles (Massonnet and Feigl, 1998; Bechor and Zebker, 2006). We applied the projection to all pixels given that no steep slope occurs on the five rock glaciers of interest. We considered the propagation of errors introduced by the InSAR measurements and DEM data which were used to determine the associated topographic parameters (Hu et al., 2021). For each interferogram, we quantified the uncertainty at the pixel level. Among all the high coherent pixels, the largest uncertainty is 9.8 cm yr^{-1}. The velocity uncertainty is therefore considered as < 10 cm yr^{-1}.

To ensure high data quality, we selected the interferograms and documented rock glacier parts meeting the following criteria as valid results for further analyses: (1) only pixels showing acceptable coherence (>0.3) are kept; (2) the coherent pixels must cover more than 40% of the landform surfaces; (3) the mean velocity of must be larger than 5 cm yr^{-1} (Wang et al., 2017). We set this empirical threshold considering the typical noise level from atmospheric delays (5 cm yr^{-1}). The interferograms and landforms that do not meet these criteria were discarded.

Step 3: Determining the velocities of the coherently moving parts as the model constraint

Field observations have revealed that multiple areas moving differentially can occur on rock glaciers and exhibit complex kinematic patterns (e.g., Buchli et al., 2018), which violates the assumption of a continuously moving body (Sect. 3.1, Fig. 3). Therefore, we aim to identify the coherently moving part of the landform that corresponds with our assumption and is thus suitable for model application.

After the procedure described in Step 2, for each selected landform, the remaining interferograms constituted a series of observations spanning multiple years. Then we defined and outlined the "coherently moving part" of each landform by considering the time series of downslope velocity of each pixel acquired during the observational periods. If the InSAR-measured velocity is higher than 5 cm yr^{-1} in more than half of the interferograms, the pixel was included in the coherently

moving part of the landform. Otherwise, the pixel is discarded, i.e., not included in the coherently moving part. The area is considered as inactive or in a transitional kinematic status.

Then, we analysed the velocity values of all pixels within the coherently moving part of the landform and selected the mean, median, and maximum values for each observation to characterise the surface kinematics of the landforms. The mean velocity error is the square root of the quadratic sum of all the velocity errors (see Code and Data Availability), which is limited to < 1cm yr^{-1}.

Finally, we take the range of the spatially averaged velocities within the coherently moving parts over the observational period as the velocity constraint for modelling ice content. By doing so, isolated patterns are neglected assuming that they may be related to short-term fluctuations, not representative of the multi-annual kinematic behaviour of the whole landform.

Table 2. List of ALOS PALSAR and ALOS-2 PALSAR-2 interferograms used in the study.

Satellite	Acquisition interval (days)	Period	Path/frame	Orbit direction	No. of interferograms
ALOS	46	Dec 2007 to Feb 2010	507/540	Ascending	8
ALOS	46	Dec 2007 to Feb 2010	507/550	Ascending	6
ALOS	46	Jun 2007 to Feb 2010	508/540	Ascending	4
ALOS	46	May 2006 to Jul 2006	511/540	Ascending	1
ALOS-2	14	Mar 2015	48/3050	Descending	1
ALOS-2	14	Jun 2015 to Feb 2020	156/550	Ascending	20

3.5.2 Deriving geometric and structural parameters from remote sensing products

Area, width, and slope angle are quantified using the same method as described in Sect. 3.3. Active layer thickness was determined as the mean value over the extent of each rock glacier, based on the 2006–2017 estimate from the European Space Agency Permafrost Climate Change Initiative Product (ESA CCI) (Obu et al., 2020). The empirical relation for calculating rock glacier thickness used in the validation procedure (Sect. 3.3) was applied here to obtain the thickness parameter. The surface velocity constraint is the range of InSAR-derived downslope velocity during the observed period; except for Tobuche rock glacier where the abnormal value in 2015 has been removed from the range (see Sect. 4.4.1 for details).

4 Results

In this section we first present the results of our model development including the calibrated parameterisation schemes (Sect. 4.1), model validation (Sect. 4.2), and model sensitivity (Sect. 4.3). Then we report the modelled ice content in Khumbu and Lhotse valleys (Sect. 4.4).
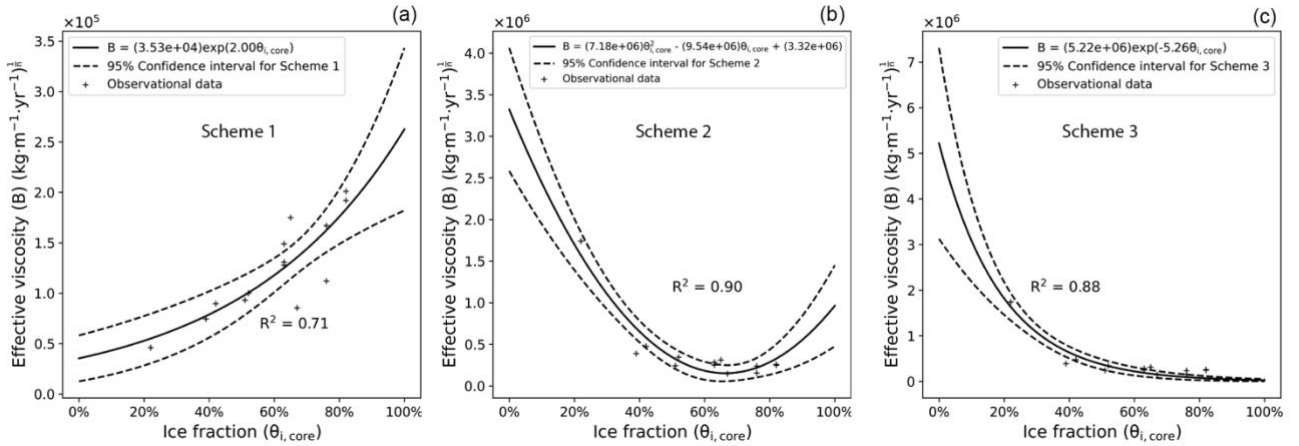
4.1 Calibrated parameterisation schemes

300 By applying the different regression models to depict the $B-\theta_{i,core}$ relationship (Fig. 4a–c), we obtained three candidate parameterisation schemes expressed as:

Scheme 1: $\qquad u_s = \dfrac{2(\rho_{al}h_{al}+\rho_{core}h_{core})^4}{\rho_{core}(n+1)}\left(\dfrac{S_f g \sin\alpha}{35300e^{2.01\theta_{i,core}}}\right)^3 ,$ (15)

Scheme 2: $\qquad u_s = \dfrac{2(\rho_{al}h_{al}+\rho_{core}h_{core})^{3\theta_{i,core}+1}}{\rho_{core}(3\theta_{i,core}+1)}\left(\dfrac{S_f g \sin\alpha}{7183435\theta_{i,core}{}^2-9543596\theta_{i,core}+3322637}\right)^{3\theta_{i,core}} ,$ (16)

Scheme 3: $\qquad u_s = \dfrac{2(\rho_{al}h_{al}+\rho_{core}h_{core})^{3\theta_{i,core}+1}}{\rho_{core}(3\theta_{i,core}+1)}\left(\dfrac{S_f g \sin\alpha}{5217905e^{-5.26\theta_{i,core}}}\right)^{3\theta_{i,core}} ,$ (17)

305

Figure 4: (a)–(c) Relationships between the ice fraction ($\theta_{i,core}$) and the effective viscosity (B) estimated from the three regression equations and parameterisation schemes (Eq. 15, 16, and 17, respectively). The observational data are derived from the GPR and DGPS measurements in Monnier and Kinnard (2015b & 2016).

4.2 Model validation

310 We simulated the surface velocities (u_s) of the three rock glaciers using Schemes 1–3. Uncertainties from the statistical analysis (dashed lines in Fig. 4) and area delineation (Sect. 3.3) have been considered in the simulation. We used the mean annual surface velocities, calculated from the Terrestrial Ground Survey data (PERMOS, 2019), as the constraint for inferring the ice content.

For each rock glacier, an inferred ice content range is derived based on the velocity constraint and modelled $u_s-\theta_{i,core}$

315 relationship. The median of the range is selected as the inferred ice content and compared with the reference ice content, i.e., the average value of the estimated ice content based on previous field measurements (Cicoira et al., 2019a; Arenson et al., 2002; Hoelzle et al., 1998).

Comparing the observed and modelled ice content from the three schemes, we see that Scheme 2 is the optimal model for the following two reasons: (1) the reference ice content is within the range inferred from Scheme 2 (Fig. 5, Fig S2 and S3); (2)

320 Scheme 2 gives the smallest root mean square error (RMSE) (8%) compared with Scheme 1 (9%) and Scheme 3 (12%) (Table 3). We used the RMSE (8%) derived from Scheme 2 to represent the uncertainty of our approach.
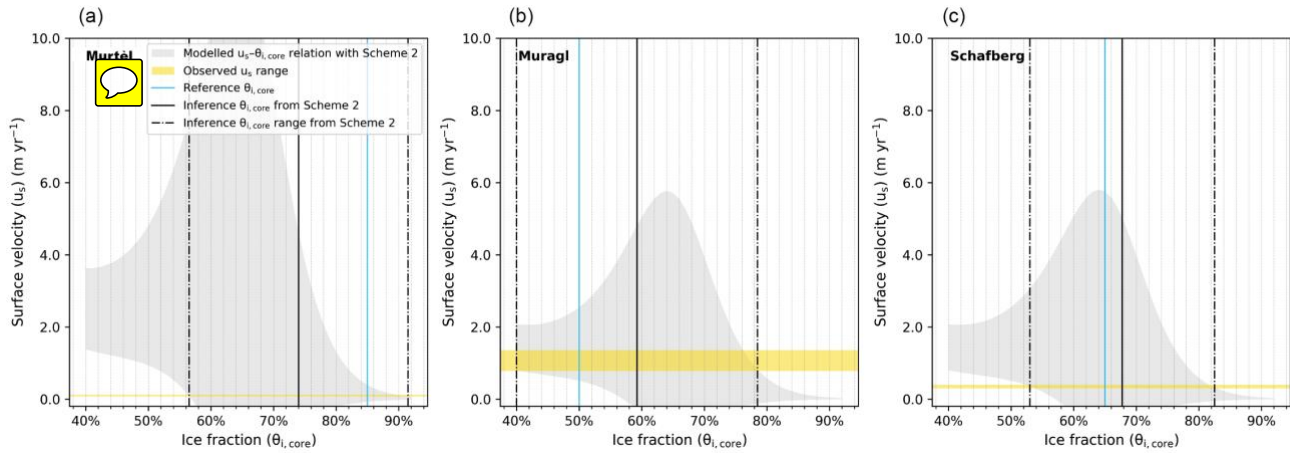

Figure 5: Modelled relationships (grey shaded areas) between the ice fraction ($\theta_{i,core}$) and the surface velocity (u_s) of 95% confidence intervals for the three RGs monitored in the PERMOS network with model parameterisation Scheme 2. The yellow bands show the
325 observed surface velocities, and the blue lines denote the reference ice contents. For each rock glacier, the intersection between the simulated $\theta_{i,core}$ - u_s relationship (grey shaded area) and the observed velocity (yellow band) gives the estimated range of ice content, as marked by the dash-dotted black lines. We take the ~~estimated~~ average as the inferred ice content ~~and show the value~~ by the solid black line.

Table 3. Summary of the reference and inference ice contents derived from the three model parameterisation schemes. The values
330 in brackets following the inference ice contents give the corresponding bias from the reference ice contents. The last row presents the root mean square error (RMSE) of the schemes.

Rock glacier	Reference (%)	Inference and bias		
		Scheme 1 (%)	Scheme 2 (%)	Scheme 3 (%)
Murtèl-Corvatsch	85	91 (6)	74 (–11)	79 (–6)
Muragl	50	56 (6)	59 (9)	66 (16)
Schafberg	65	79 (14)	68 (3)	76 (11)
RMSE	–	9	8	12

4.3 Model sensitivity

The results of sensitivity experiments are normalised to the corresponding values of the reference scenario (Scn-1.0, Fig. 6). We observe that the inference result remains stable in response to most varying parameters, with a bias of less than 5%, relative
335 to the reference scenario (Scn-1.0). The model has a higher sensitivity to the surface slope angle. In the extreme scenario (Scn-0.2), the inferred ice content can be altered by 15%. In non-extreme cases (e.g., Scn-0.8, Scn-0.6), the influences of varying slope angles can be well constrained within the 5% range. In general, the model is mostly insensitive to the uncertainties of any single input parameter.
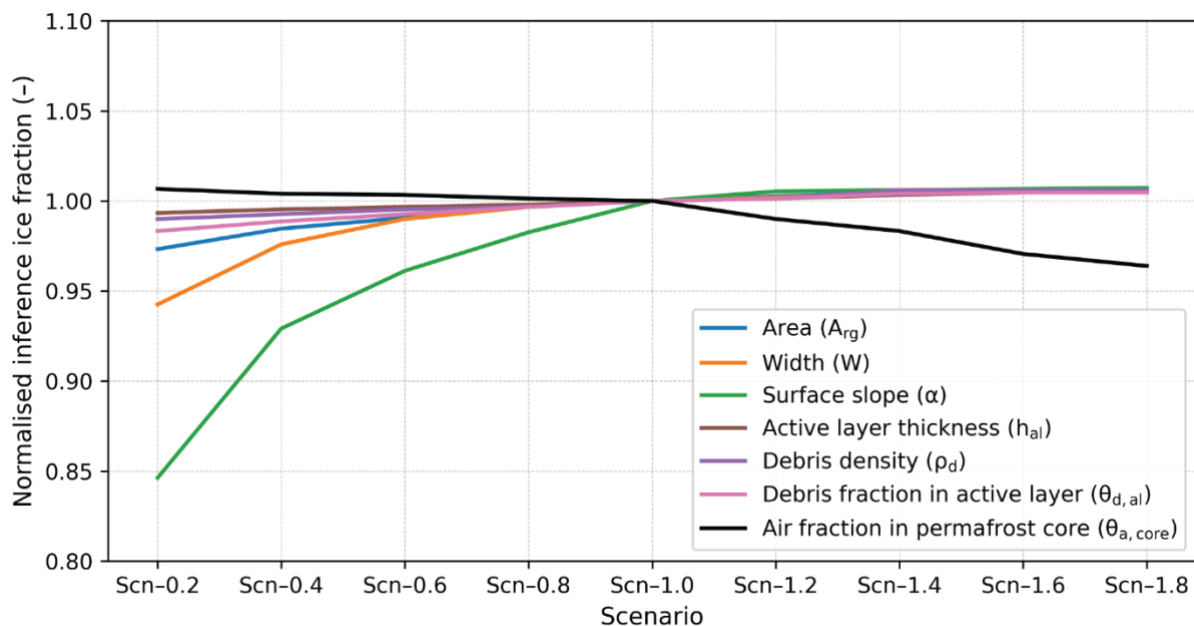
Figure 6: Normalised inference ice fractions from sensitivity experiments with different parameter scenarios. The varying parameters include rock glacier area (blue line), width (orange line), surface slope (green line), active layer thickness (brown line), debris density (purple line), debris fraction in the active layer (pink line), and air faction in permafrost core (black line).

4.4 Modelled ice contents in Khumbu and Lhotse valleys

In this subsection, we summarise the characteristics of InSAR-derived surface velocities we used as model constraints (Sect. 4.4.1) and present the modelled ice content of the five rock glaciers in the study area (Sect. 4.4.2).

4.4.1 InSAR-derived surface velocities as model constraints

We used InSAR to derive the downslope surface velocities of five rock glaciers situated in the study region. Surface velocities of the nearby debris-covered glaciers were also measured and presented in Fig. S4 and S5 in the supplementary materials.

Figure 7 shows the time series of the InSAR-derived surface velocities of the coherently moving sections of the rock glaciers. By selecting the mean velocity as the representative value, most rock glaciers, except for Tobuche, moved at a nearly constant rate, ranging from 5 cm yr^{-1} to 30 cm yr^{-1} during the observational period, with the largest standard deviation being 3.4 cm yr^{-1} for Lingten (Fig. 7d). The maximum velocity represents the local extreme of downslope rate and was as high as 112.1±12.4 cm yr^{-1} for Lingten during 2019/07/15–2019/08/26 (Fig. 7d). Tobuche displayed similar behaviour before 2010 but had accelerated more than four times from 14.9±0.2 cm yr^{-1} to 81.4±2.4 cm yr^{-1} between 2010 and 2015 (Fig. 7e). The maximum velocity reached was 181.0±57.4 cm yr^{-1} for the period 2015/03/18–2015/03/22 (Fig. 7e). However, the associated uncertainties during this period were high: the relative uncertainties of mean, median, and maximum velocity were 2.9%, 38.2%, and 31.7%, respectively. The acceleration of Tobuche cannot be confidently revealed by our data and 2015 acquisition

15

was therefore discarded from the velocity series used as the modelling constraint. The extents of coherently moving parts of the five rock glaciers are presented in Fig. 8, with the average velocities derived from the interferograms obtained during the observation period.
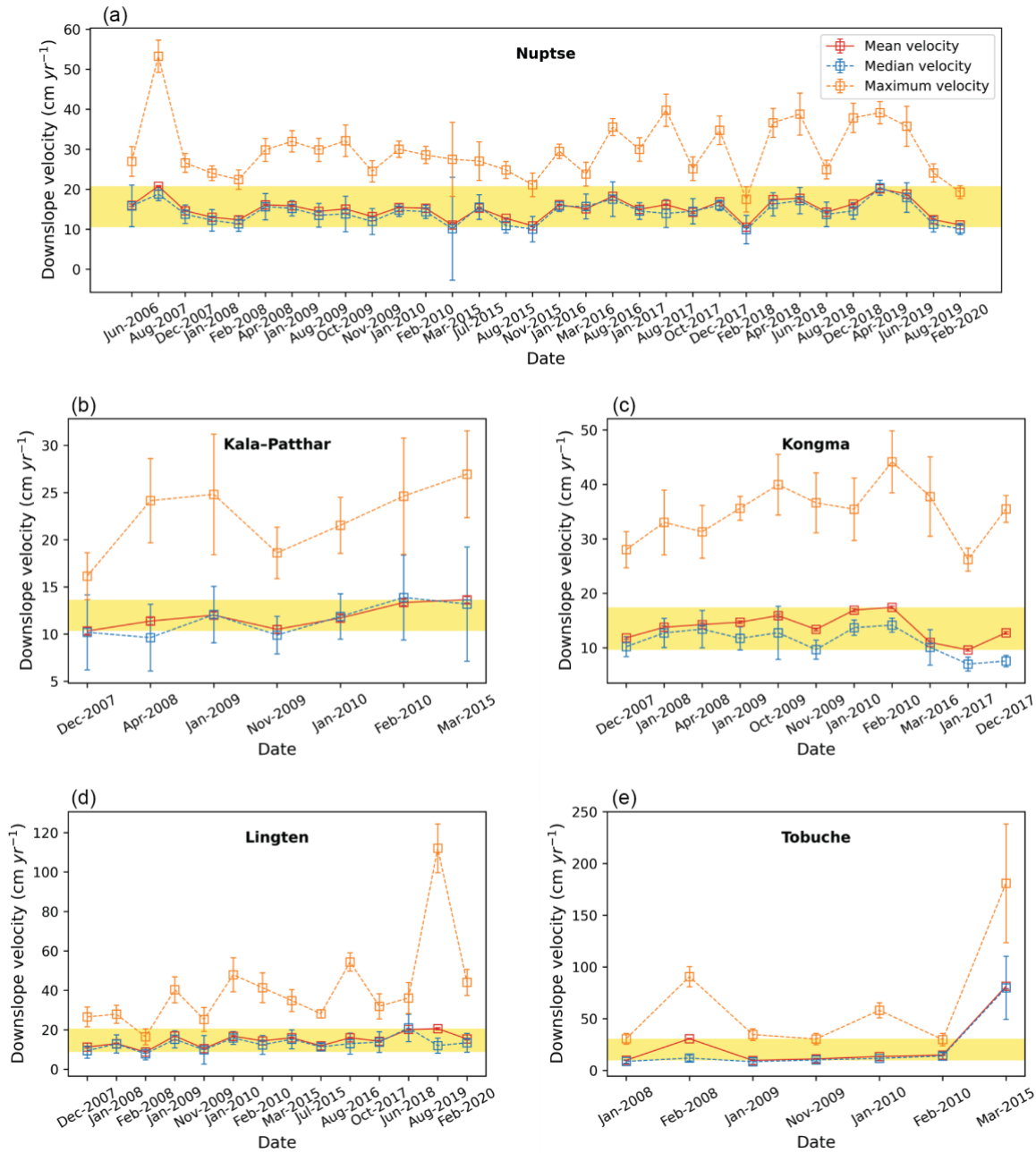
Figure 7: Time series of the InSAR-derived downslope velocities of the ~~landforms~~. The spatial mean velocities and uncertainties during each period are shown (red squares and error bars) as well as the median (blue) and maximum (orange) velocities. The yellow bands highlight the range of the mean velocities which were used as model constraints for estimating ice fractions.
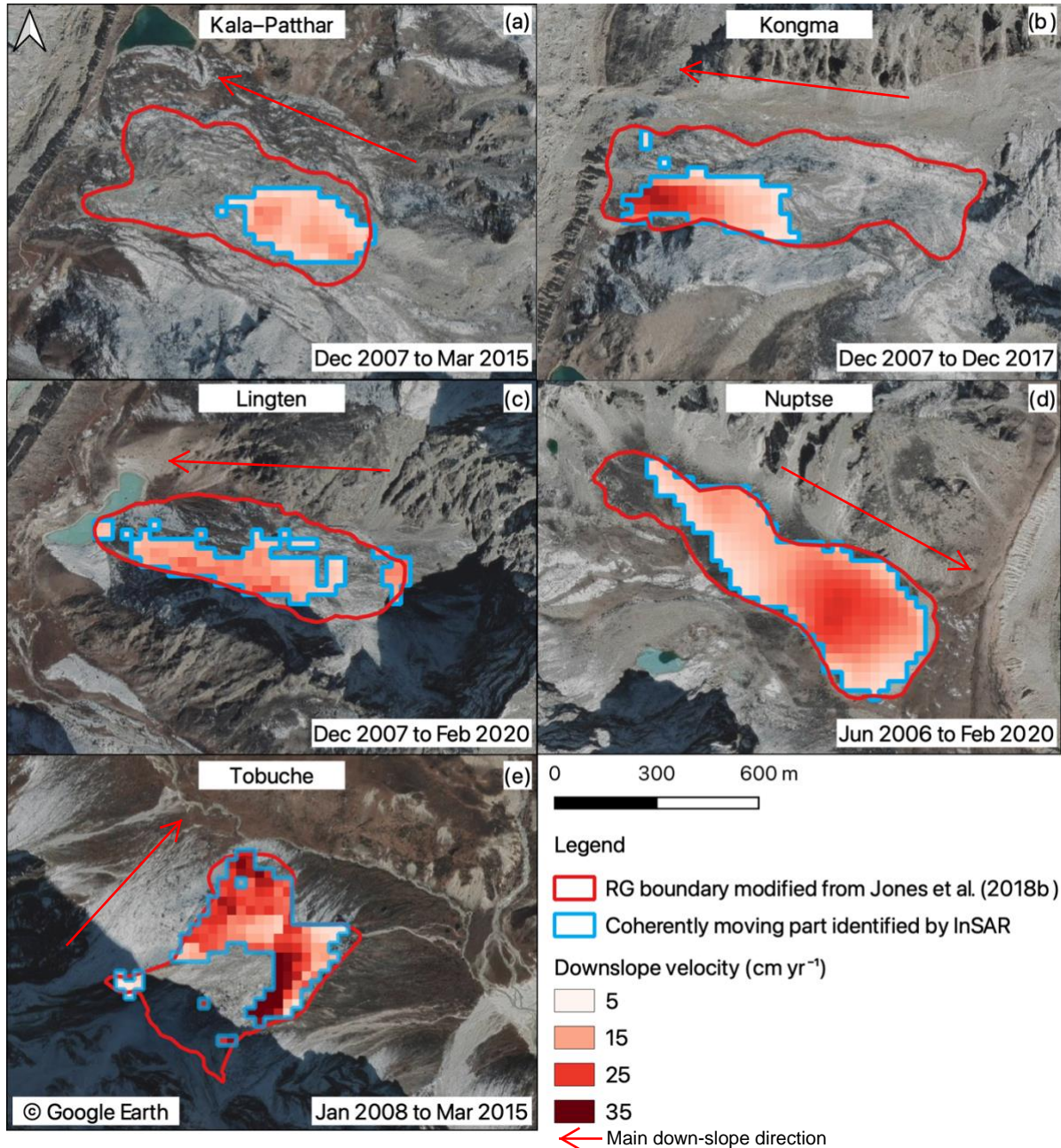
365

Figure 8: Velocity field maps show the average velocities of the coherently moving parts of the five rock glaciers (blue outlines) in the study area. The boundaries of the ~~landforms~~ delineated in Jones et al. (2018b) are in red. The transparent areas between the red and blue boundaries are due to low coherence or low velocity during the observational periods.

4.4.2 Modelled ice content

370 The geometric and structural data used as input parameters are detailed in Table 4. The five rock glaciers are tongue-shaped features and their areal extents are substantially larger than the three validation rock glaciers (Table 1 and 4). Figure 9 and Table 4 present the inference ice contents of rock glaciers based on Scheme 2 in the study area. Considering the error of the modelling results (Sect. 4.2, Table 3), the inferred average ice fractions of the coherently moving parts of the ~~landforms~~ range from 70±8% to 74±8%; the water volume equivalents of the moving parts of individual ~~landforms,~~ which are calculated based

375 on the ice fractions and the volume of the moving parts, range from 1.4±0.2 to 5.9±0.6 million m^3. Nuptse stores the most ice by volume due to its largest dimensions (Table 4). The total amount of water stored in rock glaciers in our study area lies between 12.1 and 15.1 million m^3, with an average value of 13.6 million m^3.

Table 4. Summary of the geometric and structural parameters and the inferred ice content of the coherently moving part of rock glaciers in the study area.

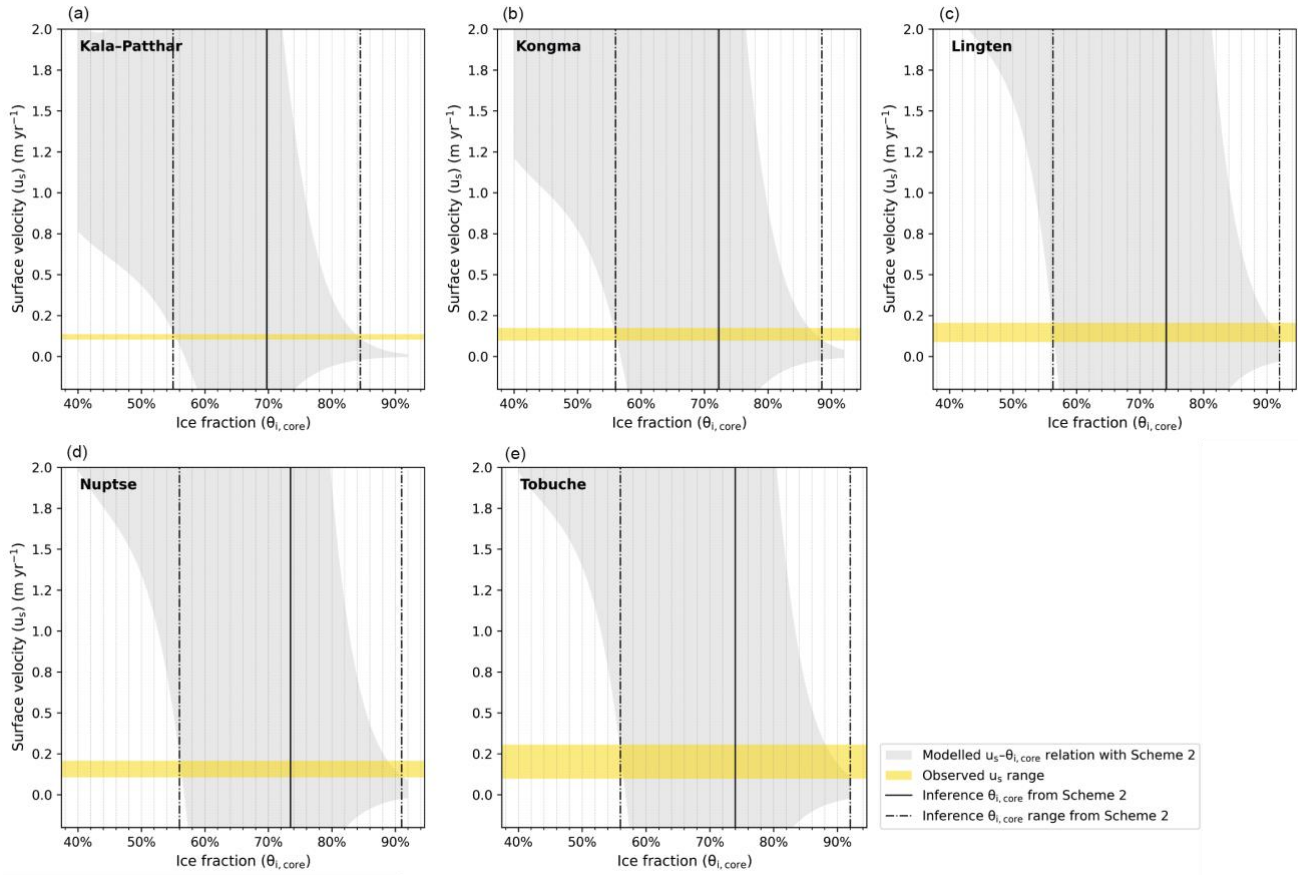| Rock glacier	Area (A_{rg}) (km^2)	Area of the coherently moving part (A_{cmp}) (km^2)	Width (W) (m)	Active layer thickness (h_{al}) (m)	Surface slope (α) (°)	Inference ice content (%)	Water volume equivalent of the coherently moving part (million m^3)
Kala-Patthar	0.275	0.074	240	0.68	9	70±8	1.4±0.2
Kongma	0.384	0.077	300	0.83	13	72±8	1.5±0.2
Lingten	0.228	0.094	240	0.65	20	74±8	5.9±0.6
Nuptse	0.310	0.234	400	0.30	13	74±8	2.0±0.2
Tobuche	0.236	0.128	400	1.67	16	74±8	2.7±0.3

380

Figure 9: Modelled relationships between the ice fraction ($\theta_{i,core}$) and the surface velocity (u_s) of 95% confidence intervals for the five RGs in Khumbu Valley with model parameterisation Scheme 2 (grey shaded areas). The ranges of the InSAR-derived velocities (yellow bands) are used as the velocity constraints for inferring ice contents from the modelled relationships. The upper and lower boundaries of the estimated ice contents are within the range outlined by the dash-dotted black lines and the solid black lines show the mean values representing the inference ice contents.

5 Discussion

In this section, we first discuss the two major sources of uncertainties in our approach, namely the amount of field data for model calibration (Sect. 5.1.1) and the derivation of rock glacier thickness (Sect. 5.1.2). Then we introduced two limitations of the model application including the incapability of predicting ground ice evolution (Sect. 5.2.1) and the limited application to rock glaciers in quasi-steady-state motion (Sect. 5.2.2). We conclude the discussion with summarizing the contribution of this study in relation to previous research and the potential improvements and application prospect of the approach (Sect. 5.3).

5.1 Major uncertainty sources

The effects of minor error sources were tested and discussed in Sect. 4.3. Here we ~~introduce~~ the two major uncertainty sources.

5.1.1 The amount of field data for model calibration

The empirical relationship between the effective viscosity and ice content is fundamental to model calibration in this study (Sect. 3.2). Currently, the amount of field data is limited for deriving the statistical relationship since detailed knowledge of rock glacier composition is largely lacking, which is the most important factor affecting the accuracy of our approach.

400 We relied on the geophysical data obtained from Las Liebres rock glacier in the Andes to calibrate the model (Monnier and Kinnard, 2015b), and hypothesized that the empirical expressions can be generalised to rock glaciers developed in a warm permafrost environment. The validation results achieved from samples in a different region, i.e., the Swiss Alps, proves the transferability of the model (Sect. 3.3). However, due to the limited amount of calibration data (14 measurements in total), the uncertainty of the derived effective viscosity–ice fraction relationship (dash lines in Fig. 4b) leads to a wide range of propagated

405 uncertainty when modelling the ice content–surface velocity relationship (grey shadings in Fig. 5). More field data are necessary to accurately represent this empirical relationship.

5.1.2 Derivation of rock glacier thickness

We discuss the uncertainty in deriving rock glacier thickness because it influences the surface velocities most significantly. As shown in Eq. 8, the surface velocity is proportional to the thickness to the power of $n + 1$, resulting from the vertical

410 integration of Eq. 7. We use the thickness–area scaling relationship (Eq. 14, Brenning, 2005a) which has also been adopted by previous research on assessing the hydrological importance of rock glaciers (e.g., Azócar and Brenning, 2010; Bodin et al., 2010; Janke et al., 2017; Jones et al., 2018, 2021; Perucca and Esper Angillieri, 2011; Rangercroft et al., 2015; Wagner et al., 2021), yet the reliability of this empirical derivation method has generated discussions (Arenson and Jakob, 2010; Brenning, 2010). Wagner et al. (2021) suggested an adapted relationship by subtracting 10 m from the derived thickness to remove the

415 likely overestimation effect. An alternative empirical method is proposed as a linear relationship between surface slope angle and thickness (Cicoira et al., 2020). We compared the estimated thickness of the validated rock glaciers from the classical thickness–area and the recently established thickness–slope relationships with the field measurements and found that the two sets of results display the same level of error (~2 m, Table S2).

In the validation part, we estimated the thickness-related error by considering the uncertainty involved in delineating the rock

420 glacier area based on Google Earth images. The uncertainties were caused by the multiple factors such as the variable image quality, the subjective judgment of operators, and the complexity of the rock glacier morphology (Brardinoni et al., 2019; Schmid et al., 2015; Way et al., 2021). We assumed a 40% uncertainty in the area parameter, leading to a ~10% error (or an absolute error of 2–4 m) in thickness. In addition, we conducted analysis assuming a more significant thickness error according to previous studies (Cicoira et al., 2020; Wagner et al., 2021), i.e., 6 m and 10 m, and obtained errors in ice content of 12%

425 and 13%, respectively, which are greater than the 8% uncertainty in our results (Fig. S7 and S8; Table S3).

In general, the uncertainty in deriving rock glacier thickness remains challenging to accurately quantify, which is primarily attributed to the insufficiency of ground truth data to build a rigorous relationship between the rock glacier thickness and

surface parameters (e.g., area, slope). In addition, rock glaciers, especially the talus-derived ones, tend to develop very variable thicknesses across the ~~landform,~~ the distribution of which cannot be inferred using the existing empirical approaches. Thus,

430 the uncertainty introduced by thickness derivation cannot be eliminated when applied to rock glaciers without known structure information.

5.2 Limitations of the model application

5.2.1 Incapability of predicting ground ice evolution

Our approach is not applicable to predict the evolution of ground ice in rock glaciers. Our results were presented in the form

435 of a modelled relationship between the ice content and surface velocity (as shown by the grey shading in Fig. 5, S2, S3 and 9), which might mislead the readers to interpret the ground ice changes from rock glacier kinematic variations. For instance, assuming the surface velocity of Kala-Patthar rock glacier reaches 1 m yr^{-1}, the corresponding ice fraction would be approximately 60% (detailed in Fig. S6 in the supplement material). However, we cannot draw the conclusion that ground ice stored in Kala-Patthar rock glacier would decrease by 10% if it accelerated to 1 m yr^{-1}, because the geometric parameters of

440 the ~~landform~~ would change accordingly, particularly the thickness of the permafrost core and the active layer, making the current modelled relationship no longer valid.

In the proposed approach, we assume that the amount of ice stored in rock glaciers remain constant within the timescale of our study (1–2 decades, constrained by InSAR data), which is consistent with the fact that rock glaciers are currently not a major contribution to surface runoff in the study area (Duguay et al., 2015; Jones et al., 2019b). Landforms undergoing rapid changes

445 in ice content and corresponding morphology, such as transitional features from glaciers to rock glaciers, are beyond the applicability of our model.

5.2.2 Limited application to rock glaciers in quasi-steady-state motion

By using the adapted form of Glen's flow law (Eq. 2), we primarily assume~~d~~ the rock glacier movement to be steady-state creep driven by viscoelastic deformation of the ice–debris mixture (Moore, 2014). This premise indicates that our method is

450 applicable to rock glaciers currently moving at a relatively constant rate. Recent research has reported abrupt and significant acceleration of rock glaciers triggered by abnormal surface warming events (Delaloye et al., 2013; Scotti et al., 2017). These destabilised rock glaciers are beyond the applicability of our method. In this study, we measure~~d~~ surface velocities of rock glaciers over multiple years to consider an average rate and avoid misleading conclusions based on ~~unrepresentative~~ short-term patterns.

455 Particularly, our model is suitable to be applied to the coherently moving part. Some parts of rock glaciers are in a transitional kinematic status (practically defined as velocities < 5 cm yr^{-1}) or behave differently from the coherently moving parts. The 1-D InSAR method may fail to detect some moving areas of the ~~landforms~~ creeping nearly along the satellite's flight direction

due to the lack of sensitivities of the LOS geometry. These parts may also contain ice but are excluded from our estimation, causing possible underestimation of ground ice storage.

460 Additionally, the motion of rock glaciers affected by significant subsidence (instead of or in addition to downslope creep) cannot be measured accurately, due to the limitation of 1-D InSAR method: we converted the LOS measurements to surface velocities by assuming the rock glacier moves downslope without additional subsidence component.

5.3 Contribution and prospect of the approach

For the first time, we build a model framework to infer ice content with remote sensing-based input by taking advantage of the
465 existing observational data. Previous research either relied on costly and labor-intensive in-situ methods, such as borehole drilling and geophysical surveys, to measure the ice content of individual rock glaciers (e.g., Haeberli et al., 1998; Hauck, 2013), or provided categorized estimates for regional scale studies (e.g., Jones et al., 2018 and 2021). The approach we have developed makes it possible to more conveniently and quantitatively assess the ground ice stored in individual or even region-wide rock glaciers.

470 The proposed approach can be further improved. The likely emergence of more data to be integrated for model calibration and validation, will allow for improving the accuracy of the method. A more accurate 2-D surface velocity can be obtained by using multi-track InSAR data (e.g., Bertone et al., 2022; Zhang et al., 2021), allowing us to apply the model to rock glaciers with a complex velocity field. We expect the improved model can be valuably applied to mountain permafrost regions where rock glaciers are widespread for preliminary water storage evaluation.

475 ## 6 Conclusions

We developed an empirical rheological model for inferring ice content of the coherently moving parts of rock glaciers and apply it to estimate the water storage of rock glaciers situated in the Khumbu and Lhotse Valleys using surface velocities derived from InSAR measurements. The main findings are summarised as follows:

(1) An empirical rheological model is presented in this study for estimating ice content of rock glaciers using five input
480 parameters, namely rock glacier area, width, surface slope angle, active layer thickness, and surface velocity, all of which can be obtained from readily available remote sensing products or forthcoming datasets.

(2) Mean downslope velocities in the coherently moving parts of the rock glaciers situated in Khumbu and Lhotse Valleys ranged from 5 cm yr^{-1} to 30 cm yr^{-1} and mostly remained constant during the observational period (2006–2020).

(3) The inferred average ice contents of rock glaciers in Khumbu and Lhotse Valleys ranges from 70±8% to 74±8%; the water
485 volume equivalent ranges from 1.4 to 5.9 million m^3 for individual landforms, Nuptse rock glacier stores the most ice due to its largest dimensions among the five studied rock glaciers. Total amount of water stored in the five rock glaciers in Khumbu and Lhotse Valleys ranges from 12.1±0.2 to 15.1±0.6 million m^3, with an average value of 13.6 million m^3.

This study develops an approach to inferring ice content of rock glaciers by using surface-velocity-constrained model. The estimated ice content and water storage in the study area confirms the hydrological significance of rock glaciers in the Nepalese

490 Himalaya. We argue that the model shows great promise ~~in being able to assess~~ ice storage in rock glaciers although more field data are needed to improve the reliability of this initial modelling framework.

Code and data availability

The source code of ISCE is available at https://github.com/isce-framework/isce2. The ALOS PALSAR and ALOS-2 PALSAR-2 data are copyrighted and provided by the Japan Aerospace Exploration Agency through the EO-RA2 project ER2A2N081.

495 Data for the rock glacier kinematics in the Swiss Alps are available at http://www.permos.ch/data.html. The ESA CCI permafrost data are available at http://catalogue.ceda.ac.uk/uuid/1f88068e86304b0fbd34456115b6606f. The code of the modelling approach for estimating ice content will be provided by Yan Hu upon request.

Author contribution

YH developed the code, performed the data analysis and interpretation, visualised the results, and wrote the majority of the

500 manuscript. SH conceptualised the research goal, supervised the study, and wrote Sect. 1 of the draft. LL advised YH and actively helped the investigation process. JLW helped formulate the initial framework of the method and collect research data. All the authors contributed to the reviewing and editing of the manuscript.

Competing interests

The authors declare that they have no conflict of interest.

References

Arenson, L., Hoelzle, M., and Springman, S.: Borehole deformation measurements and internal structure of some rock glaciers in Switzerland, Permafrost Periglac., 13, 117-135, https://doi.org/10.1002/ppp.414, 2002.

515 Arenson, L., and Springman, S.: Mathematical descriptions for the behaviour of ice-rich frozen soils at temperatures close to 0 C, Can. Geotech. J., 42, 431-442, https://doi.org/10.1139/t04-109, 2005a.

Arenson, L., and Springman, S.: Triaxial constant stress and constant strain rate tests on ice-rich permafrost samples, Can. Geotech. J., 42, 412-430, https://doi.org/10.1139/t04-111, 2005b.

Arenson, L. U., and Jakob, M.: The significance of rock glaciers in the dry Andes – A discussion of Azócar and Brenning (2010) and
520 Brenning and Azócar (2010), Permafrost and Periglacial Processes, 21, 282-285, 10.1002/ppp.693, 2010.

Azizi, F., and Whalley, W. B.: Numerical modelling of the creep behaviour of ice-debris mixtures under variable thermal regimes, in: International Offshore and Polar Engineering Conference Proceedings, The Sixth International Offshore and Polar Engineering Conference, Los Angeles, 1996, WOS:A1996BF95F00053, 362-366,

Azócar, G. F., and Brenning, A.: Hydrological and geomorphological significance of rock glaciers in the dry Andes, Chile (27°-33°S),
525 Permafrost Periglac., 21, 42-53, https://doi.org/10.1002/ppp.669, 2010.

Ballantyne, C. K.: Periglacial geomorphology, John Wiley & Sons, Hoboken, NJ, USA, 2018.

Barsch, D., Fierz, H., and Haeberli, W.: Shallow core drilling and borehole measurements in the permafrost of an active rock glacier near the Grubengletscher, Wallis, Swiss Alps, Arctic Alpine Res., 11, 215-228, https://doi.org/10.2307/1550646, 1979.

Bechor, N. B. D. and Zebker, H. A.: Measuring two-dimensional movements using a single InSAR pair, Geophys Res Lett, 33,
530 https://doi.org/10.1029/2006gl026883, 2006.

Berthling, I., Etzelmüller, B., Isaksen, K., and Sollid, J. L.: Rock glaciers on Prins Karls Forland. II: GPR soundings and the development of internal structures, Permafrost Periglac., 11, 357-369, https://doi.org/10.1002/1099-1530, 2000.

Berthling, I.: Beyond confusion: Rock glaciers as cryo-conditioned landforms, Geomorphology, 131, 98-106, https://doi.org/10.1016/j.geomorph.2011.05.002, 2011.

535 Bertone, A., Barboux, C., Bodin, X., Bolch, T., Brardinoni, F., Caduff, R., Christiansen, H. H., Darrow, M. M., Delaloye, R., Etzelmüller, B., Humlum, O., Lambiel, C., Lilleøren, K. S., Mair, V., Pellegrinon, G., Rouyet, L., Ruiz, L., and Strozzi, T.: Incorporating InSAR kinematics into rock glacier inventories: insights from 11 regions worldwide, Cryosphere, 16, 2769–2792, https://doi.org/10.5194/tc-16-2769-2022, 2022.

Bodin, X., Rojas, F., and Brenning, A.: Status and evolution of the cryosphere in the Andes of Santiago (Chile, 33.5°S.), Geomorphology, 118, 453-464, https://doi.org/10.1016/j.geomorph.2010.02.016, 2010.

Brardinoni, F., Scotti, R., Sailer, R., and Mair, V.: Evaluating sources of uncertainty and variability in rock glacier inventories, Earth Surf Processes, 44, 2450–2466, https://doi.org/10.1002/esp.4674, 2019.

Brenning, A.: Geomorphological, hydrological and climatic significance of rock glaciers in the Andes of Central Chile (33-35 degrees S), Permafrost Periglac., 16, 231-240, https://doi.org/10.1002/ppp.528, 2005a.

Brenning, A.: Climatic and geomorphological controls of rock glaciers in the Andes of Central Chile, Humboldt-Universität zu Berlin, Mathematisch-Naturwissenschaftliche Fakultät II, 2005b.

Brenning, A.: The significance of rock glaciers in the dry Andes – reply to L. Arenson and M. Jakob, Permafrost and Periglacial Processes, 21, 286-288, 2010.

Buchli, T., Kos, A., Limpach, P., Merz, K., Zhou, X. H., and Springman, S. M.: Kinematic investigations on the Furggwanghorn Rock Glacier, Switzerland, Permafrost Periglac., 29, 3-20, https://doi.org/10.1002/ppp.1968, 2018.

Carslaw, H. S., and Jaeger, J. C.: Conduction of heat in solids, Oxford Science Publications. Clarendon Press, Oxford, 1959.

Chen, C. W., and Zebker, H. A.: Phase unwrapping for large SAR interferograms: statistical segmentation and generalized network models, IEEE T. Geosci Remote., 40, 1709-1719, https://doi.org/10.1109/TGRS.2002.802453, 2002.

Cicoira, A., Beutel, J., Faillettaz, J., Gartner-Roer, I., and Vieli, A.: Resolving the influence of temperature forcing through heat conduction on rock glacier dynamics: a numerical modelling approach, The Cryosphere, 13, 927-942, https://doi.org/10.5194/tc-13-927-2019, 2019a.

Cicoira, A., Beutel, J., Faillettaz, J., and Vieli, A.: Water controls the seasonal rhythm of rock glacier flow, Earth Planet Sc. Lett., 528, https://doi.org/10.1016/j.epsl.2019.115844, 2019b.

Cicoira, A., Marcer, M., Gärtner-Roer, I., Bodin, X., Arenson, L. U., and Vieli, A.: A general theory of rock glacier creep based on in-situ and remote sensing observations, Permafrost Periglac., https://doi.org/10.1002/ppp.2090, 2020.

Corte, A.: The Hydrological Significance of Rock Glaciers, J. Glaciol., 17, 157-158, https://doi.org/10.3189/s0022143000030859, 1976.

Croce, F. A., and Milana, J. P.: Internal structure and behaviour of a rock glacier in the Arid Andes of Argentina, Permafrost Periglac., 13, 289-299, https://doi.org/10.1002/ppp.431, 2002.

Cuffey, K., and Paterson, W. S. B.: The physics of glaciers, 4th ed., Butterworth-Heinemann/Elsevier, Burlington, MA, 2010.

Delaloye, R., Morard, S., Barboux, C., Abbet, D., Gruber, V., Riedo, M., and Gachet, S.: Rapidly moving rock glaciers in Mattertal, Geogr. Helv., 21-31, 2013.

Duguay, M. A., Edmunds, A., Arenson, L. U., and Wainstein, P. A.: Quantifying the significance of the hydrological contribution of a rock glacier–A review, GeoQuébec 2015, 2015.

Frehner, M., Ling, A. H. M., and Gärtner-Roer, I.: Furrow-and-ridge morphology on rockglaciers explained by gravity-driven buckle folding: A case study from the Murtèl rockglacier (Switzerland), Permafrost Periglac., 26, 57-66, https://doi.org/10.1002/ppp.1831, 2015.

570   Fujii, Y., and Higuchi, K.: Ground Temperature and its Relation to Permafrost Occurrences in the Khumbu Region and Hidden Valley, Journal of Japanese Society of Snow and Ice., 38, 125-128, https://doi.org/10.5331/seppyo.38.Special_125, 1976.

Fukui, K., Fujii, Y., Ageta, Y., & Asahi, K.: Changes in the lower limit of mountain permafrost between 1973 and 2004 in the Khumbu Himal, the Nepal Himalayas. *Global and Planetary Change*, *55*(4), 251–256. https://doi.org/10.1016/j.gloplacha.2006.06.002, 2007.

Geiger, S. T., Daniels, J. M., Miller, S. N., and Nicholas, J. W.: Influence of Rock Glaciers on Stream Hydrology in the La Sal Mountains,
575   Utah, Arctic, Antarctic, and Alpine Research, 46, 645-658, https://doi.org/10.1657/1938-4246-46.3.645, 2014.

Glen, J. W.: The creep of polycrystalline ice, Proceedings of the Royal Society of London. Series A, Mathematical and Physical Sciences (1934-1990), 228, 519-538, https://doi.org/10.1098/rspa.1955.0066, 1955.

Guglielmin, M., Camusso, M., Polesello, S., and Valsecchi, S.: An old relict glacier body preserved in permafrost environment: The Foscagno rock glacier ice core (Upper Valtellina, Italian central Alps), Arctic AntArctic Alpine Res., 36, 108-116, https://doi.org/10.1657/1523-0430,
580   2004.

Haeberli, W., Hoelzle, M., Kaab, A., Keller, F., Vonder Mühll, D., and Wagner, S.: Ten years after drilling through the permafrost of the active rock glacier Murtél, Eastern Swiss Alps: answered questions and new perspectives, Seventh International Conference on Permafrost, Yellowknife, 1998, 403-410,

Haeberli, W.: Modern research perspectives relating to permafrost creep and rock glaciers: A discussion, Permafrost Periglac., 11, 290-293,
585   https://doi.org/10.1002/1099-1530(200012)11:4, 2000.

Hanssen, R. F.: Radar interferometry : data interpretation and error analysis, edited by: NetLibrary, I., Kluwer Academic, Dordrecht Boston, 2001.

Hauck, C.: New concepts in geophysical surveying and data interpretation for permafrost terrain, Permafrost Periglac., 24, 131-137, https://doi.org/10.1002/ppp.1774, 2013.

590   Hausmann, H., Krainer, K., Bruckl, E., and Mostler, W.: Internal structure and ice content of reichenkar rock glacier (Stubai alps, Austria) assessed by geophysical investigations, Permafrost Periglac., 18, 351-367, https://doi.org/10.1002/ppp.601, 2007.

Hoelzle, M., Wagner, S., Kääb, A., and Vonder Mühll, D.: Surface movement and internal deformation of ice-rock mixtures within rock glaciers in the Upper Engadin, Switzerland, Proceedings of the 7th International Conference on Permafrost, 465-471, 1998.

Hu, Y., Liu, L., Wang, X., Zhao, L., Wu, T., Cai, J., Zhu, X., and Hao, J.: Quantification of permafrost creep provides kinematic evidence
595   for classifying a puzzling periglacial landform, Earth Surf Proc Land., 46, 465-477, https://doi.org/10.1002/esp.5039, 2021.

Jakob, M.: Active rock glaciers and the lower limit of discontinuous alpine permafrost, Khumbu-Himalaya, Nepal, Permafrost Periglac., 3,
253-256, 1992.

Janke, J. R., Ng, S., and Bellisario, A.: An inventory and estimate of water stored in firn fields, glaciers, debris-covered glaciers, and rock
glaciers in the Aconcagua River Basin, Chile, Geomorphology, 296, 142-152, https://doi.org/10.1016/j.geomorph.2017.09.002, 2017.

600   Jones, D. B., Harrison, S., Anderson, K., and Betts, R. A.: Mountain rock glaciers contain globally significant water stores, Sci Rep., 8,
https://doi.org/10.1038/s41598-018-21244-w, 2018a.

Jones, D. B., Harrison, S., Anderson, K., Selley, H. L., Wood, J. L., and Betts, R. A.: The distribution and hydrological significance of rock
glaciers in the Nepalese Himalaya, Global Planet Change., 160, 123-142, https://doi.org/10.1016/j.gloplacha.2017.11.005, 2018b.

Jones, D. B., Harrison, S., and Anderson, K.: Mountain glacier-to-rock glacier transition, Global Planet Change., 181,
605   https://doi.org/10.1016/j.gloplacha.2019.102999, 2019a.

Jones, D. B., Harrison, S., Anderson, K., and Whalley, W. B.: Rock glaciers and mountain hydrology: A review. *Earth-Science Reviews,
193*, 66-90. https://doi.org/10.1016/j.earscirev.2019.04.001, 2019b.

Jones, D. B., Harrison, S., Anderson, K., Shannon, S., and Betts, R. A.: Rock glaciers represent hidden water stores in the Himalaya, Sci.
Total Environ., 145368, https://doi.org/10.1016/j.scitotenv.2021.145368, 2021.

610   Kääb, A., Frauenfelder, R., and Roer, I.: On the response of rockglacier creep to surface temperature increase, Global Planet Change., 56,
172-187, https://doi.org/10.1016/j.gloplacha.2006.07.005, 2007.

Kenner, R., Pruessner, L., Beutel, J., Limpach, P., and Phillips, M.: How rock glacier hydrology, deformation velocities and ground
temperatures interact: Examples from the Swiss Alps, Permafrost Periglac., 31, 3-14, https://doi.org/10.1002/ppp.2023, 2019.

Kneisel, C., Hauck, C., Fortier, R., and Moorman, B.: Advances in geophysical methods for permafrost investigations, Permafrost Periglac.,
615   19, 157-178, https://doi.org/10.1002/ppp.616, 2008.

Knight, J., Harrison, S., and Jones, D. B.: Rock glaciers and the geomorphological evolution of deglacierizing mountains, Geomorphology,
324, 14-24, https://doi.org/10.1016/j.geomorph.2018.09.020, 2019.

Krainer, K., Bressan, D., Dietre, B., Haas, J. N., Hajdas, I., Lang, K., Mair, V., Nickus, U., Reidl, D., Thies, H., and Tonidandel, D.: A
10,300-year-old permafrost core from the active rock glacier Lazaun, southern Ötztal Alps (South Tyrol, northern Italy), Quaternary Res.,
620   83, 324-335, https://doi.org/10.1016/j.yqres.2014.12.005, 2015.

Krainer, K., and Mostler, W.: Hydrology of Active Rock Glaciers: Examples from the Austrian Alps, Arctic, Antarctic, and Alpine Research, 34, 142-149, https://doi.org/10.1080/15230430.2002.12003478, 2002.

Ladanyi, B.: Rheology of ice/rock systems and interfaces, The Eighth International Conference on Permafrost, Zurich, Switzerland, 2003, WOS:000185049300110, 621-626,

625   Leopold, M., Williams, M. W., Caine, N., Völkel, J., and Dethier, D.: Internal structure of the Green Lake 5 rock glacier, Colorado Front Range, USA, Permafrost Periglac., 22, 107-119, https://doi.org/10.1002/ppp.706, 2011.

Liu, L., Millar, C. I., Westfall, R. D., and Zebker, H. A.: Surface motion of active rock glaciers in the Sierra Nevada, California, USA: inventory and a case study using InSAR, Cryosphere, 7, 1109–1119, https://doi.org/10.5194/tc-7-1109-2013, 2013.

Massonnet, D. and Feigl, K. L.: Radar interferometry and its application to changes in the Earth's surface, Rev Geophys, 36, 441–500,
630   https://doi.org/10.1029/97rg03139, 1998.

Mellor, M., and Testa, R.: Effect of temperature on the creep of ice, J. Glaciol., 8, 131-145, 1969.

Monnier, S., and Kinnard, C.: Internal structure and composition of a rock glacier in the Andes (upper Choapa valley, Chile) using borehole information and ground-penetrating radar, Ann. Glaciol., 54, 61-72, https://doi.org/10.3189/2013AoG64A107, 2013.

Monnier, S., and Kinnard, C.: Reconsidering the glacier to rock glacier transformation problem: New insights from the central Andes of
635   Chile, Geomorphology, 238, 47-55, https://doi.org/10.1016/j.geomorph.2015.02.025, 2015a.

Monnier, S., and Kinnard, C.: Internal structure and composition of a rock glacier in the Dry Andes, Inferred from ground-penetrating radar data and its artefacts, Permafrost Periglac., 26, 335-346, https://doi.org/10.1002/ppp.1846, 2015b.

Monnier, S., and Kinnard, C.: Interrogating the time and processes of development of the Las Liebres rock glacier, central Chilean Andes, using a numerical flow model, Earth Surf Proc Land., 41, 1884-1893, 10.1002/esp.3956, 2016.

640   Moore, P. L.: Deformation of debris-ice mixtures, Rev. Gepphys., 52, 435-467, https://doi.org/10.1002/2014rg000453, 2014.

Munroe, J. S.: Distribution, evidence for internal ice, and possible hydrologic significance of rock glaciers in the Uinta Mountains, Utah, USA, Quaternary Res., 90, 50-65, https://doi.org/10.1017/qua.2018.24, 2018.

Nan, Z., Li, S., and Liu, Y.: Mean annual ground temperature distribution on the Tibetan plateau: Permafrost distribution mapping and further application, Journal of Glaciology and Geocryology, 24, 142-148, 2002.

645   Obu, J.; Westermann, S.; Barboux, C.; Bartsch, A.; Delaloye, R.; Grosse, G.; Heim, B.; Hugelius, G.; Irrgang, A.; Kääb, A.M.; Kroisleitner, C.; Matthes, H.; Nitze, I.; Pellet, C.; Seifert, F.M.; Strozzi, T.; Wegmüller, U.; Wieczorek, M.; Wiesmann, A.: ESA Permafrost Climate

Change Initiative (Permafrost_cci): Permafrost version 2 data products. Centre for Environmental Data Analysis, *date of citation*. http://catalogue.ceda.ac.uk/uuid/1f88068e86304b0fbd34456115b6606f, 2020

Oerlemans, J.: Glaciers and climate change, A.A. Balkema Publishers, Lisse, 2001.

650 PERMOS: Permafrost in Switzerland 2014/2015 to 2017/2018, edited by: Noetzli, J., Luethi, R., and Staub, B., the Cryospheric Commission of the Swiss Academy of Sciences, Glaciological Report (Permafrost) No. 12–15, 104 pp., 2019.

Perucca, L., and Esper Angillieri, M. Y.: Glaciers and rock glaciers' distribution at 28° SL, Dry Andes of Argentina, and some considerations about their hydrological significance, Environmental Earth Sciences, 64, 2079-2089, 10.1007/s12665-011-1030-z, 2011.

Pruessner, L., Huss, M., Phillips, M., and Farinotti, D.: A framework for modeling rock glaciers and permafrost at the basin-scale in high
655 alpine catchments, Journal of Advances in Modeling Earth Systems, 13, e2020MS002361, 2021.

Rangecroft, S., Harrison, S., Anderson, K., Magrath, J., Castel, A. P., and Pacheco, P.: A first rock glacier inventory for the Bolivian Andes, Permafrost Periglac., 25, 333-343, https://doi.org/10.1002/ppp.1816, 2014.

Rangecroft, S., Harrison, S., and Anderson, K.: Rock Glaciers as Water Stores in the Bolivian Andes: An Assessment of Their Hydrological Importance, Arctic, Antarctic, and Alpine Research, 47, 89-98, 10.1657/AAAR0014-029, 2015.

660 Reinosch, E., Gerke, M., Riedel, B., Schwalb, A., Ye, Q., and Buckel, J.: Rock glacier inventory of the western Nyainqêntanglha Range, Tibetan Plateau, supported by InSAR time series and automated classification, Permafrost Periglac, 32, 657–672, https://doi.org/10.1002/ppp.2117, 2021.

RGIK: Towards standard guidelines for inventorying rock glaciers: baseline concepts (version 4.2.2), http://rgik.org, 2021.

RGIK – baseline concepts: Towards standard guidelines for inventorying rock glaciers: baseline concepts (Version 4.2.2), IPA Action Group
665 Rock   glacier   inventories   and   kinematics,   3,   https://bigweb.unifr.ch/Science/Geosciences/Geomorphology/ Pub/Website/IPA/Guidelines/V4/220331_Baseline_Concepts_ Inventorying_Rock_Glaciers_V4.2.2.pdf, last access: 16 May 2022.

Rouyet, L., Lauknes, T. R., Christiansen, H. H., Strand, S. M., and Larsen, Y.: Seasonal dynamics of a permafrost landscape, Adventdalen, Svalbard, investigated by InSAR, Remote Sens Environ, 231, 111236, https://doi.org/10.1016/j.rse.2019.111236, 2019.

Salerno, F., Guyennon, N., Thakuri, S., Viviano, G., Romano, E., Vuillermoz, E., Cristofanelli, P., Stocchi, P., Agrillo, G., Ma, Y., and
670 Tartari, G.: Weak precipitation, warm winters and springs impact glaciers of south slopes of Mt. Everest (central Himalaya) in the last 2 decades (1994–2013), The Cryosphere, 9, 1229-1247, https://doi.org/10.5194/tc-9-1229-2015, 2015.

Schmid, M.-O., Baral, P., Gruber, S., Shahi, S., Shrestha, T., Stumm, D., and Wester, P.: Assessment of permafrost distribution maps in the Hindu Kush Himalayan region using rock glaciers mapped in Google Earth, Cryosphere, 9, 2089–2099, https://doi.org/10.5194/tc-9-2089-2015, 2015.

675   Scott, W. J., Sellmann, P. V., and Hunter, J. A.: Geophysics in the study of permafrost, in: Geotechnical and Environmental Geophysics: Volume I, Review and Tutorial, 355-384, 1990.

Scotti, R., Crosta, G. B., and Villa, A.: Destabilisation of Creeping Permafrost: The Plator Rock Glacier Case Study (Central Italian Alps), Permafrost Periglac, 28, 224–236, https://doi.org/10.1002/ppp.1917, 2017.

Steig, E. J., Fitzpatrick, J. J., Potter, j. N., and Clark, D. H.: The geochemical record in rock glaciers, Geogr. Ann. A., 80, 277-286, 680   https://doi.org/10.1111/j.0435-3676.1998.00043.x, 1998.

Wagner, T., Kainz, S., Helfricht, K., Fischer, A., Avian, M., Krainer, K., and Winkler, G.: Assessment of liquid and solid water storage in rock glaciers versus glacier ice in the Austrian Alps, Science of The Total Environment, 800, 149593, https://doi.org/10.1016/j.scitotenv.2021.149593, 2021.

Wang, X., Liu, L., Zhao, L., Wu, T., Li, Z., and Liu, G.: Mapping and inventorying active rock glaciers in the northern Tien Shan of China 685   using satellite SAR interferometry, Cryosphere, 11, 997–1014, https://doi.org/10.5194/tc-11-997-2017, 2017.

Way, R. G., Wang, Y., Bevington, A. R., Bonnaventure, P. P., Burton, J. R., Davis, E., Garibaldi, M. C., Lapalme, C. M., Tutton, R., Wehbe, M. A.E.: Consensus-Based Rock Glacier Inventorying in the Torngat Mountains, Northern Labrador. American Society of Civil Engineers Proceedings. Regional Conference on Permafrost and the 19th International Conference on Cold Regions Engineering. https://doi.org/10.31223/X5C60W, 2021.

690   Whalley, W. B., and Azizi, F.: Rheological models of active rock glaciers - evaluation, critique and a possible test, Permafrost Periglac., 5, 37-51, https://doi.org/10.1002/ppp.3430050105, 1994.

Wirz, V., Gruber, S., Purves, R. S., Beutel, J., Gärtner-Roer, I., Gubler, S., & Vieli, A.: Short-term velocity variations at three rock glaciers and their relationship with meteorological conditions. *Earth Surface Dynamics*, *4*(1), 103–123. https://doi.org/10.5194/esurf-4-103-2016, 2016.

695   Zhang, X., Feng, M., Zhang, H., Wang, C., Tang, Y., Xu, J., Yan, D., and Wang, C.: Detecting rock glacier displacement in the Central Himalayas using multi-temporal InSAR, Remote Sensing, 13, 4738, https://doi.org/10.3390/rs13234738, 2021.

Zhao, L., and Sheng, Y.: Permafrost survey manual, Science Press, Beijing, 2015.

Supplements for

Modelling rock glacier velocity and ice content based on InSAR-derived velocity, Khumbu and Lhotse Valleys, Nepal

Yan Hu[1,2,3], Stephan Harrison[2], Lin Liu[1,3], Joanne Laura Wood[2]

[1]Earth System Science Programme, Faculty of Science, The Chinese University of Hong Kong, Hong Kong SAR, China
[2]College of Life and Environmental Sciences, University of Exeter, Penryn, Cornwall, TR10 9EZ, UK
[3]Institute of Environment, Energy and Sustainability, The Chinese University of Hong Kong, The Chinese University of Hong Kong, Hong Kong SAR, China

Correspondence to: Yan Hu (huyan@link.cuhk.edu.hk)

Contents of this file

Table S1, S2, and S3; Figures S1, S2, S3, S4, S5, S6, S7, and S8
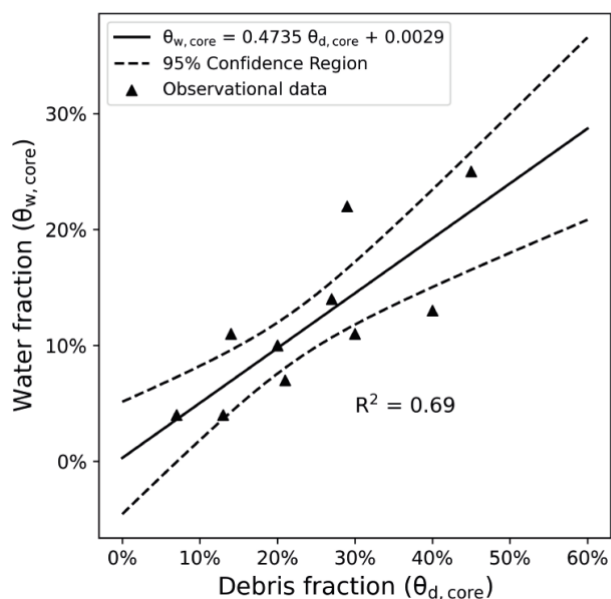
Figure S1: Relationship between debris fraction ($\theta_{d,core}$) and water fraction ($\theta_{w,core}$). The observational data are derived from the GPR and DGPS measurements in Monnier and Kinnard (2015b & 2016).

Table S1. Parameters of the sensitivity experiments. Scn-1.0 is the reference scenario that adopts the parameters of Murtèl-Corvatsch rock glacier. The other scenarios are designed by multiplying the reference value of each variable with the corresponding factor in their scenario labels.

Scenario	A_{rg} (km²)	W (m)	α (°)	h_{al} (m)	ρ_d (kg/m³)	$\theta_{d,al}$ (%)	$\theta_{a,core}$ (%)
Scn-0.2	0.01297	40	3.2	0.6	1450	13	1.5
Scn-0.4	0.02594	80	6.4	1.2	1700	26	3.0
Scn-0.6	0.03892	120	9.6	1.8	1950	39	4.5
Scn-0.8	0.05189	160	12.8	2.4	2200	52	6.0
Scn-1.0	0.06487	200	16	3.0	2450	65	7.5
Scn-1.2	0.07784	240	19.2	3.6	2700	72	9.0
Scn-1.4	0.09081	280	22.4	4.2	2950	79	10.5
Scn-1.6	0.10379	320	25.6	4.8	3200	86	12.0
Scn-1.8	0.11677	360	28.8	5.4	3450	93	13.5

20
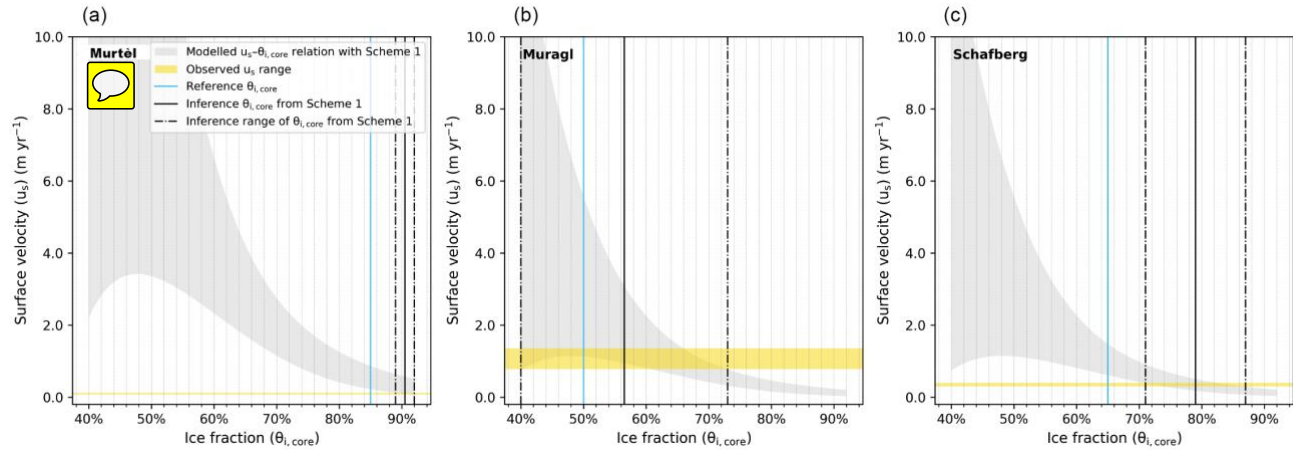
Figure S2: Modelled relationships (grey shaded areas) between the ice fraction ($\theta_{i,core}$) and the surface velocity (u_s) of 95% confidence intervals for the three RGs monitored in the PERMOS network with model parameterisation Scheme 1. The ranges of the observed velocities (yellow bands) are used as velocity constraints for inferring ice content from the modelled relationships. Also shown are the reference ice content obtained from previous field-based surveys (blue lines). The inference ice contents are the mean values (solid black lines) with the estimated ranges (dash-dotted black lines).
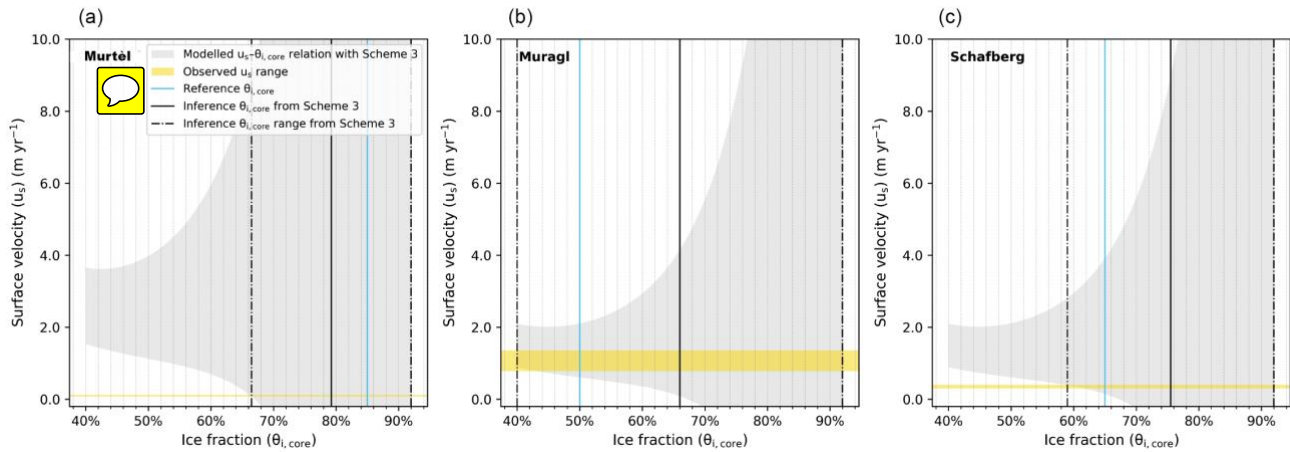
2

Figure S3: Similar to Fig. S4, but showing results derived from model parameterisation Scheme 3. The grey shaded areas outline the modelled relationships between the ice fraction ($\theta_{i,core}$) and the surface velocity (u_s) with 95% confidence intervals. The yellow bands show the observed surface velocities, and the blue lines denote the reference ice contents. For each rock glacier, the intersection between the simulated $\theta_{i,core}$- u_s relationship (grey shaded area) and the observed velocity (yellow band) gives the estimated range of ice content, as marked by the dash-dotted black lines. The inferred ice content is taken as the average value of the estimated range and indicated by the solid black line.

The debris–covered glaciers (DCGs) investigated in this study show a discontinuous and inconsistent velocity field due to its heterogeneous and fast motion which is unfavourable for InSAR measurements (Fig. S4). Figure S5 presents that the DCGs exhibit similar and stable kinematic features in mean and median velocities as rock glaciers, yet Chola DCG shows a standard deviation in mean velocity as 15.4 cm yr⁻¹, much higher than that of the rock glaciers (3.4 cm yr⁻¹). The maximum velocity is variable with the largest value of 215.9±29.7 cm yr⁻¹, as shown in Chola DCG (Fig. S5-b). However, those statistics of velocity distribution of debris-covered glaciers based on InSAR cannot characterise the heterogeneous kinematic behaviours of the entire landform because of the spatially incomplete record, as illustrated in Fig. S4.
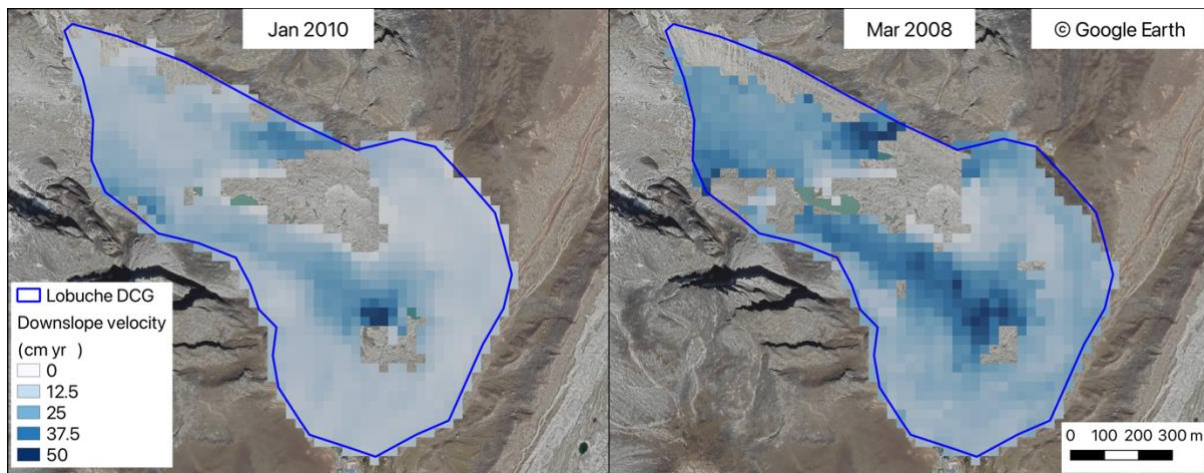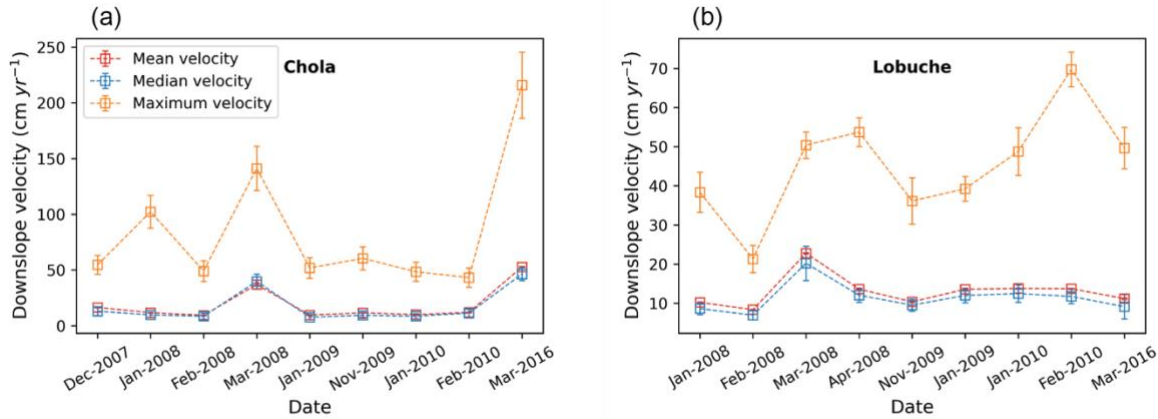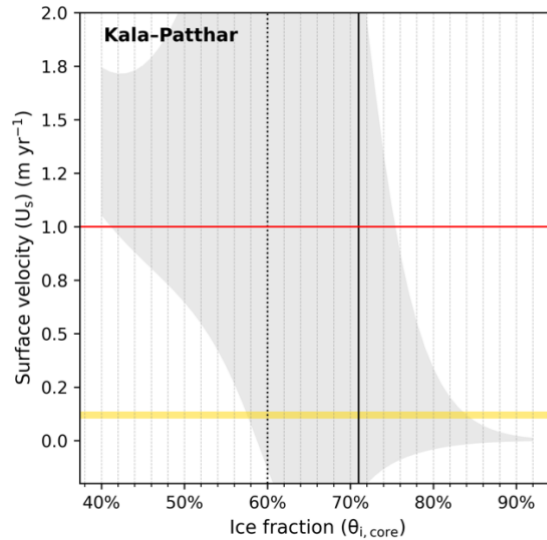
(a)
(b)

Figure S5: Time series of the InSAR-derived downslope velocities of the two debris-covered-glaciers. The spatial mean velocities and uncertainties during each period are shown (black squares and error bars) as well as the median (blue) and maximum (red) velocities.


Figure S6: Modified after Fig. 11a in the manuscript. The yellow shading shows the observed surface velocity (~0.1 m yr^{-1}) and the vertical solid black line denotes the modelled ice content (71%). The red shading marks an assumed surface velocity (1 m yr^{-1}) and the estimated ice fraction is shown by the vertical dotted line (60%).

Table S2: Estimated rock glacier thickness (T_{area}) derived from the thickness–area relationship used in this study, and the corresponding bias relative to in situ measured thickness (T_{ref}) (Barsch et al., 1979; Cicoira et al., 2019a; Arenson et al., 2002; Hoelzle et al., 1998). The rock glacier thickness (T_{slp}) derived from thickness–slope angle relationship proposed by Cicoira et al. (2020), and the associated bias. The last row gives the mean absolute error (MAE) derived from the two methods.

Rock glacier	T_{area} (m)	T_{slp} (m)	T_{ref} (m)
Murtèl-Corvatsch	29	26.2	27
Muragl	24	19	20
Schafberg	24	20.8	25
MAE	2.3	2	–
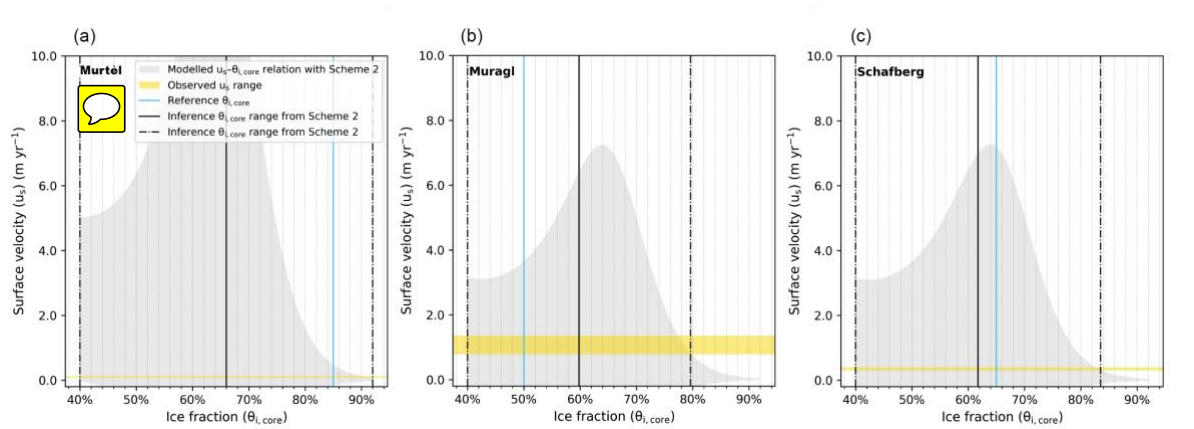
Figure S7: Modelled relationships (grey shaded areas) between the ice fraction ($\theta_{i,core}$) and the surface velocity (u_s) of 95% confidence intervals for the three RGs monitored in the PERMOS network assuming a thickness error of 6 m. The ranges of the observed velocities (yellow bands) are used as velocity constraints for inferring ice content from the modelled relationships. Also shown are the reference ice content obtained from previous field-based surveys (blue lines). The inference ice contents are the mean values (solid black lines) with the estimated ranges (dash-dotted black lines).
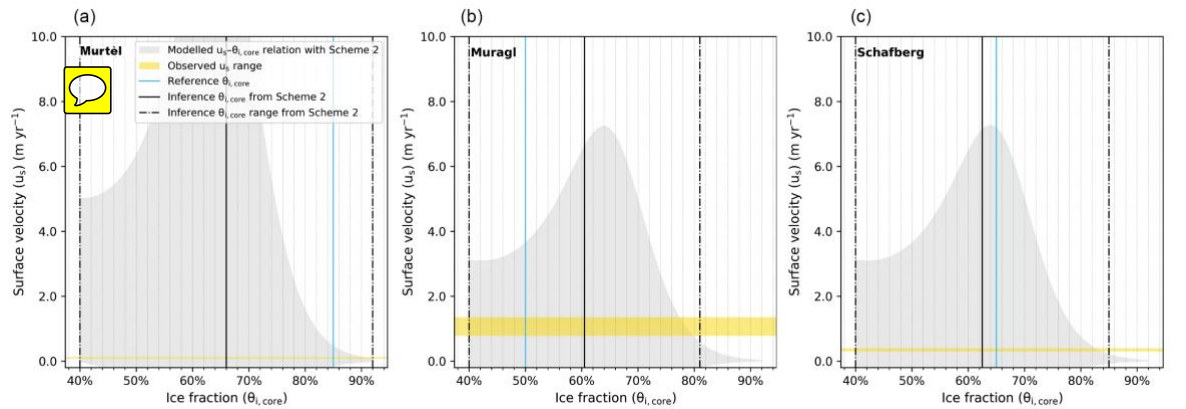
Figure S8: Similar to Fig. S7, but showing results with a thickness error of 10 m.

Table S3. Summary of the reference and inference ice contents derived from two scenarios assuming different thickness errors, namely 6 m and 10 m. The values in brackets following the inference ice contents give the corresponding bias from the reference ice contents. The last row presents the root mean square error (RMSE) of the two scenarios.

Rock glacier	Reference (%)	Inference and bias (%)	
		6-m thickness error	10-m thickness error
Murtèl-Corvatsch	85	66 (-19)	66 (-19)
Muragl	50	60 (10)	61 (11)
Schafberg	65	62 (-3)	63 (-2)
RMSE	–	12	13

6